NOVEMBER 2025

RENEWABLE ENERGY, BIOMASS & SUSTAINABILITY

ISSN: 2683-2658 Vol. 7, No. 2

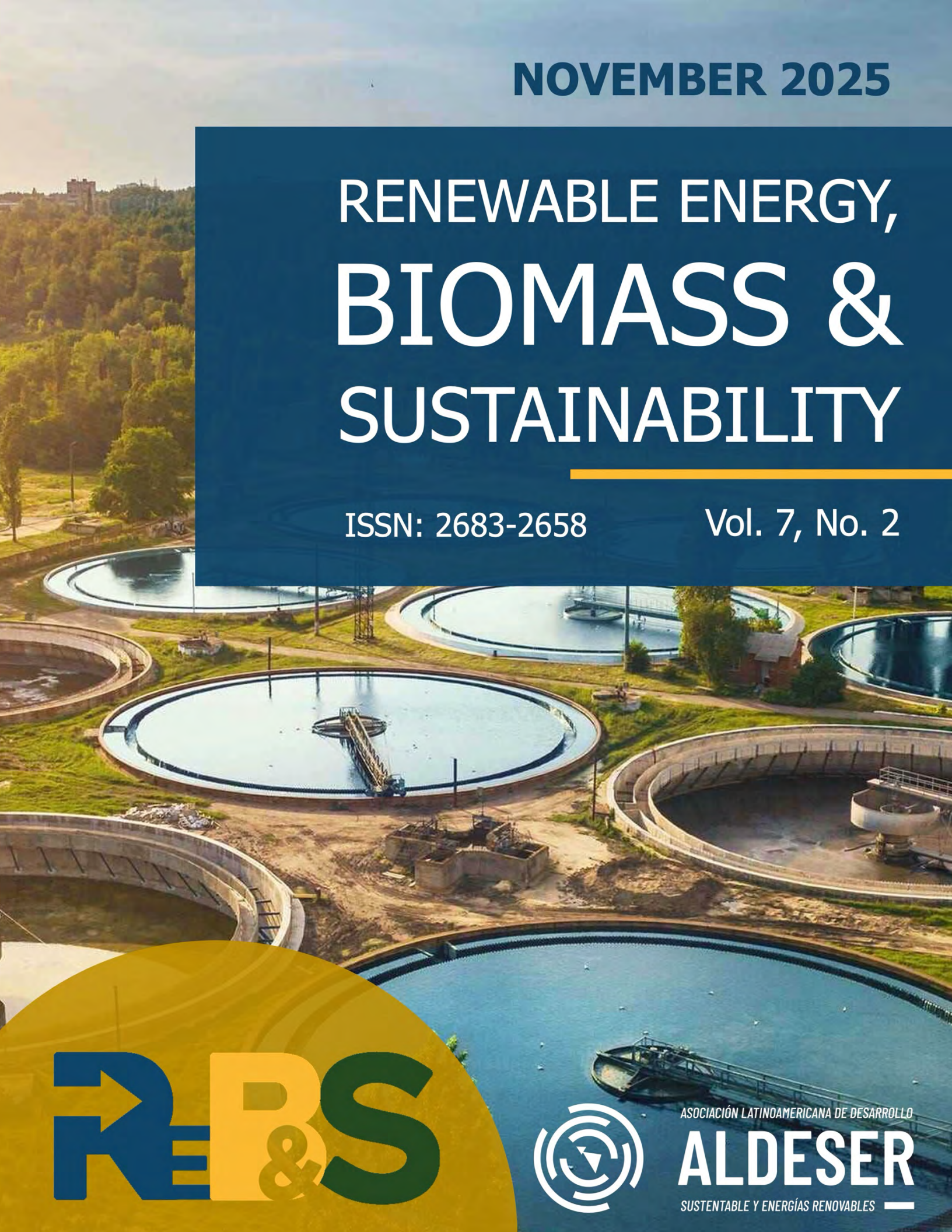

RE&S

ASOCIACIÓN LATINOAMERICANA DE DESARROLLO
ALDESER
SUSTENTABLE Y ENERGÍAS RENOVABLES

Renewable Energy, Biomass & Sustainability
Vol. 7 No. 2 (2025)

Published: September 22, 2025

Renewable Energy, Biomass & Sustainability, Vol. 7, No. 2, November 2025, is a biannual publication, published and edited by Asociación Latinoamericana de Desarrollo Sustentable y Energías Renovables A.C. (ALDESER), Sur 4 No. 270, Colonia Centro, C.P. 94300, Orizaba, Veracruz, Mexico, Tel. 2722372285, Web Page: https://aldeser.org/revistas.html and email address: secretariat@aldeser.org.

The Reservation of Rights of Exclusive Use Certificate No.: 04-2025-060617423800-102, ISSN: 2683-2658, are both granted by the Instituto Nacional del Derecho de Autor (INDAUTOR, Mexico). Responsible for the last update of this issue: Andrea Alvarado Vallejo. Date of last modification, December 16, 2025.

Table of Contents

Correlation of changes in rheological properties with the growth kinetics of *Haematococcus pluvialis* in municipal wastewater

Uriel Carmona-Rosas [1], Roger Emmanuel Sales-Pérez [1], Joaquín Estrada-García [1], Eduardo Hernández-Aguilar [2] and Juan Manuel Méndez-Contreras [1,*]

[1] División de Estudios de Posgrado e Investigación, Tecnológico Nacional de México, Instituto Tecnológico de Orizaba, Orizaba, Veracruz, México
[2] Facultad de Ciencias Químicas, Universidad Veracruzana, Prol. De Ote. 6 número 1009, Colonia Rafael Alvarado. Orizaba, Veracruz. 94340. México
* Corresponding author: juan.mc@orizaba.tecnm.mx

Received: July 31, 2025 Accepted: September 3, 2025 Published: September 22, 2025
DOI: https://doi.org/10.56845/rebs.v7i2.566

Abstract: The objective of this research was to evaluate the biodegradation of municipal wastewater through the cultivation of *Haematococcus pluvialis* in a 4-L airlift photobioreactor over a period of 14 days, establishing the relationship between growth kinetics and changes in the rheological properties of the medium as a potential process monitoring strategy. To identify the ideal inoculum percentage, a unifactorial experimental design was implemented, where tests were conducted at different levels to determine statistically significant differences between them based on the biodegradation of organic matter. Three inoculum levels (5, 10, and 15%) were analyzed in 400 mL photobioreactors where cell growth, total COD, soluble COD, and pH were monitored. Once in the airlift photobioreactor, changes in shear stress and apparent viscosity were monitored in a range of 0.1–200 rpm, along with cell density growth and pollutant degradation (total COD, soluble COD, total nitrogen, and total phosphorus) every 2 days for 14 days. Laboratory-scale experiments showed soluble COD removals exceeding 95%, with the 15% inoculum level statistically showing the highest organic load removal. In the airlift reactor scale-up, a soluble COD removal percentage of 78% was achieved, and concentrations and concentrations values below the maximum permissible limits established by Mexican regulations (NOM-001-SEMARNAT-2021) were obtained for phosphorus and nitrogen content. The rheological monitoring showed an affinity to the Herschel–Bulkley model ($R^2 > 0.99$), with a decreasing trend observed in the consistency index (k), which decreased from 8.517×10^{-5} to 1.453×10^{-5}, and an increasing trend in the flow index(n), which rose from 1.583 to 1.905. This improvement is attributed to the reduction of soluble COD to values as low as 180 mg/L and to the increase in microalgal biomass, which reached up to 1.3×10^7 cells/mL.

Keywords: Wastewater; *H. Pluvialis*; Rheological properties; Airlift reactor.

Introduction

In Mexico, the increasing generation of municipal wastewater constitutes a highly relevant environmental and public health problem. It is estimated that 76.8% (215.5 m^3/s) of the wastewater generated was collected in sewage systems, of which more than 40% does not receive adequate treatment before being discharged into receiving bodies of water (CONAGUA, 2022), which significantly contributes to the pollution of rivers, lakes, and aquifers. This situation is aggravated by the limited efficiency of conventional treatment technologies, which present technical and operational restrictions in the face of the increasing organic load and the presence of inorganic nutrients such as nitrogen and phosphorus that cause eutrophication of the environment. Furthermore, these systems usually require high energy demands because, in most cases, they require long periods of time to decompose complex organic compounds, which limits their effectiveness (Rout *et al*., 2021).

Another major problem is that these processes generate polluting byproducts; for example, activated sludge systems produce large volumes of residual sludge that require additional stabilization, dehydration, and final disposal processes (Wu *et al*., 2022), which pose environmental risks if not properly managed. On the other hand, conventional biological treatment generates greenhouse gases, mainly carbon dioxide (CO_2), nitrogen oxides (NO_x), and methane (CH_4) derived from the decomposition of organic matter. Taken together, these problems limit long-term sustainability and increase the need for new treatment alternatives (Singh *et al*., 2017).

Given this scenario, wastewater treatment with microalgae has emerged as a promising alternative in wastewater bioremediation processes due to its ability to assimilate organic and inorganic compounds, generate oxygen through photosynthesis, and produce value-added biomass. In particular, *Haematococcus pluvialis* is a green microalga of high biotechnological interest that has demonstrated a remarkable affinity for nutrients such as phosphorus and nitrogen, as well as efficient biomass accumulation under controlled cultivation conditions during its vegetative phase (Pan *et al*., 2021). This species is known for its production of extracellular polysaccharides (EPS), which can induce significant

transformations in the rheological properties inside photobioreactors, in addition to promoting the aggregation and sedimentation of suspended and colloidal compounds (Laroche, 2022; Wang *et al*., 2019). While it has been shown that microalgae can grow in open environments, to obtain higher yields and better quality biomass, it is suggested that their propagation be carried out in isolated reactors. The airlift type is an ideal configuration to promote gentle but effective mixing without the need for moving parts; its hydraulic dynamics favor the homogenization of the culture, improving the transfer of gases such as CO_2 and O_2 (Uyar *et al*., 2024). Furthermore, it keeps the microalgal cells in suspension, reducing dead zones, preventing cell damage from shear stress, and improving the overall efficiency of the process. These particular conditions of controlled flow and continuous aeration can directly affect the rheological properties of the culture because as cell density increases and biomolecules such as EPS accumulate, the apparent viscosity of the medium can increase, altering the flow profile (Adesanya *et al*., 2012).

Previous studies have shown that microbial and algal growth in alternative biodegradation systems for wastewater and semi-solid waste can influence the rheological properties of culture media, suggesting their potential as indirect monitoring tools (Gutiérrez-Casiano *et al*., 2022; Estrada-García *et al*., 2023). However, the relationship between rheology and growth kinetics in *Haematococcus pluvialis* has not been thoroughly investigated, particularly under the complex conditions of municipal wastewater, which present both high organic load and compositional variability.

In this context, this study proposes the use of rheological characterization as a control and monitoring strategy for the treatment of municipal wastewater with H. pluvialis, linking rheological changes to cell growth dynamics and the reduction of organic load. It is proposed that changes in rheological properties, particularly in parameters such as the consistency index (k) and the flow index (n) of the Herschel-Bulkley model, may be correlated with increased cell density and the efficiency of removing dissolved organic matter (soluble and total COD). This approach not only allows for a better understanding of the system's physical-biological dynamics, but it can also represent a practical and non-invasive alternative for real-time operational decision-making.

Materials and Methods

Physicochemical and microbiological characterization of Municipal Wastewater (MWW)

Sampling was carried out using NMX-AA-003-1980 in a wastewater effluent within the flow of the "Rio Blanco" located in the municipality of Mendoza, Veracruz, Mexico, with a weekly frequency and during the season known as the winter drought in the period October-December. Physicochemical and microbiological characterization of municipal wastewater (MWW) was carried out to determine its composition and contaminant potential. Sampling was maintained until the physicochemical and microbiological parameters showed consistent values between consecutive samples, with standard deviations within narrow ranges. This criterion was considered indicative of a constant composition, ensuring a representative and characteristic profile of municipal wastewater during the winter dry season.

The characterization of the wastewater consisted of determining soluble COD (COD_s) and total COD (COD_T) using the method of standard NMX-AA-030/1_SCFI-2012; the content of total solids (TS) and total volatile solids (TVS), total nitrogen (TN) using the Kjeldahl method and total phosphorus (TP) were evaluated according to the Standard Methods for the Examination of Water and Wastewater 23rd Edition (2017) (APHA *et al*., 2017), and the determination of pH by the potentiometric method.

Experiments on the growth of H. Pluvialis

The microalga *H. pluvialis* was acquired from the company Algae Bank. Initially, the alga was propagated in M1B5 medium until a concentration of approximately 7.5 x 10^6 cells/mL was reached, sufficient to begin the adaptation and growth experiments in MWW (Radice *et al*., 2024). Figure 1 shows the experimental setup for the growth of *H. pluvialis* in MWW. To evaluate the efficiency of the bioremediation process, three inoculum levels (5%, 10%, and 15%) were established in 400 mL photobioreactors with three replicates for each (n=4).

Photobioreactors with different inoculum levels were maintained under constant aeration conditions of 1.2 L/min, constant temperature (20 ± 2 °C), and white light at 1000 lux in 12:12 (light:dark) photoperiods. All experiments were monitored every 3 days for a 14-day period, during which the following parameters were tracked: COD_T, COD_s, pH, and

cell count. To identify the optimal inoculum percentage in the 400 mL photobioreactor trials, a unifactorial experimental design was implemented, in which tests were carried out at different levels to determine statistically significant differences among them based on the biodegradation of organic matter. Minitab 18.1 software was used for the statistical analysis.

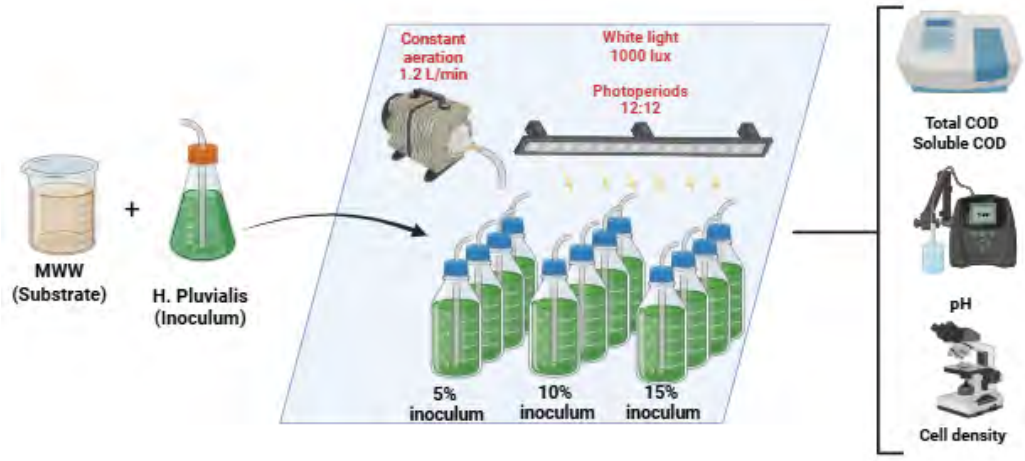

Figure 1. Bioconversion experiments using *H. Pluvialis.*

Cell density determination was performed using a Neubauer chamber, which has a central 1 mm² grid with 25 squares, each composed of 16 smaller squares. Its standard depth with the coverslip is 0.1 mm, taking into account the volume of the central quadrant: 1 mm² * 0.1 mm = 0.1 mm³ = 10^{-4} mL. Therefore, cell density was determined using Equation 1, taking into account that 25 squares were counted for greater accuracy, and the dilution factor was added as needed.

$$cell\ density\ \left[\frac{cells}{mL}\right] = \frac{number\ of\ cells * 250\ 000}{number\ of\ squares} = number\ of\ cells * 10\ 000 \quad \textbf{(1)}$$

Scaling up in airlift photobioreactors

The scaling up of experiments with *H. pluvialis* was carried out in a self-made airlift photobioreactor with a total volume of 5.5 L and a functional volume of 4 L. Figure 2 shows the design of the photobioreactor, where commonly used design parameters can be identified. It has been demonstrated that the correct proportion ratios favor efficient mixing, a homogeneous environment, and healthy cultivation without the need for mechanical agitation (Zhang *et al.*, 2014). The main column has a height of 68 cm (h_c). The main column has a height of 68 cm (h_c). The section where the gas and liquid are injected and rise is called the riser, which consists of an internal concentric tube with a diameter of 0.75 in (d_{dt}) and a height of 51 cm (h_{dt}). This tube, called the draft tube, was strategically placed 5 cm from the bottom of the photobioreactor (h_{bc}) to allow fluid recirculation. The gas sparger was located in this area and operated at a flow rate of 1.2 L/min.

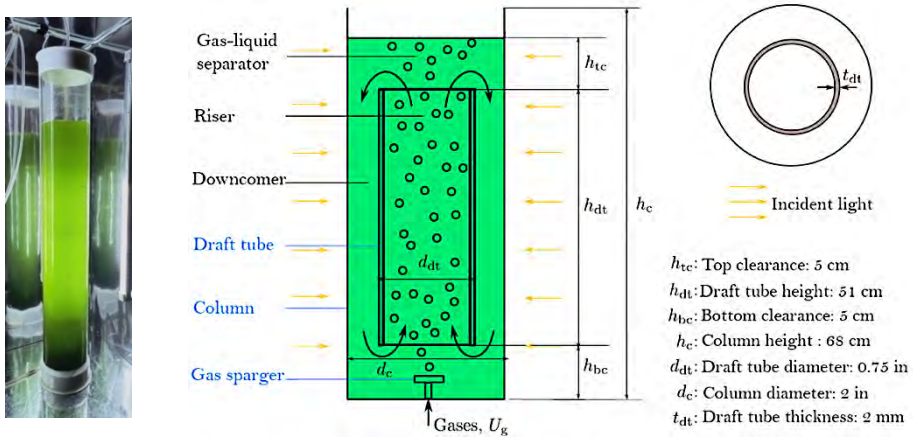

Figure 2. Design and photo of the photobioreactor used in the process. Adapted from (Li *et al.*, 2022)

At the top of the photobioreactor, a distance of 5 cm (h_{tc}) was established between the top of the inner concentric tube and the liquid level. In this area, the gas bubbles introduced to generate agitation and flow rise and are released, resulting in a physical separation between the liquid medium (microalgae) and the unabsorbed gas. For this reason, this area is called the gas-liquid separator zone (Behin & Amiri, 2023). In the part where there is no gas flow, the liquid descends by gravity due to the density difference with the ascending zone; this zone is called the downcomer zone (Mazziero *et al*., 2022).

To determine the inoculum percentage for scale-up in the airlift photobioreactor, the selected criterion was the ability to achieve the maximum permissible limits of soluble COD (sCOD) removal in the shortest possible time within the evaluated period (14 days), while simultaneously avoiding potential inhibition derived from excessive inoculum loads. The light, ventilation, and temperature conditions remained the same as in the previous phase. Samples were taken every 48 hours for 14 days to analyze the behavior of COD_T, COD_S, TN , TP, cell count, and rheological variables.

Rheological variable monitoring was performed using a Brookfield DV2T rotational viscometer with the ULA spindle. Viscosity (cP), torque (%), shear stress (Pa), and shear rate (s^{-1}) values were recorded at different angular velocities, initially in 1 rpm intervals up to 10 rpm, and subsequently from 10 rpm to 200 rpm. Shear stress was plotted against shear rate to generate rheograms; these results were then fitted to the Herschel-Bulkley, Ostwald-de Waele, and Newtonian rheological models (Equations 2-4). From these equations, rheological parameters were obtained, such as the consistency index (k), the flow index (n), the yield stress (τ_0), and the apparent viscosity (Pa·s).

$$\tau = k \cdot \dot{\gamma}^n \quad \textbf{(2)}$$

$$\tau = \tau_0 + (k \cdot \dot{\gamma}^n) \quad \textbf{(3)}$$

$$\tau = \eta \cdot \dot{y} \quad \textbf{(4)}$$

Results and Discussion

The results of the physicochemical characterization of the municipal wastewater are shown in Table 1. It should be noted that the pH can be considered neutral; this is due to several factors such as the presence of organic acids and bases in the municipal wastewater, fostered by microbiological activity with aerobic and anaerobic bacteria which produce carbonic acid and ammonia, causing a natural equilibrium tending to self-regulate the medium at a neutral pH (Huang *et al*., 2021). The pH value obtained in this study is within the range reported by Pérez-Guzmán *et al*. (2024), who mention that for municipal effluents the pH reached a value of 8.19; this parameter in both cases remained within the permissible range according to Mexican regulations (NOM-001-SEMARNAT-2021).

Table 1. Physicochemical characterization of municipal wastewater.

Parameter	Units	Average value MWW	Standard deviation
pH	-	7.90	±0.23
TS	mg/L	2066	±160
VTS	mg/L	1701	±145
COD	mg/L	2592	±324
Soluble COD	mg/L	785	±123
TP	mg/L	17	±2
TN	mg/L	32	±4

The wastewater showed high values of COD_T and COD_S (2595 mg/L and 785 mg/L respectively), which is attributed to the dry season during which the samples were taken. Both values were above the maximum permissible limit, as were the total suspended solids, indicating a high organic load. The values obtained are similar to those reported by Ata *et al*. (2021), where average COD values of 2367 mg/L were reached in the June–November period and the sampling points were located at the inlet of untreated water from different treatment plants.

A TN concentration of 32 mg/L was obtained, which is within the range of 30-35 mg/L reported in the literature for municipal wastewater (Tang *et al*., 2023). The amount of TN is directly related to the urea content in human urine, which is a typical component in the composition of this effluent and increases the nitrogen present, mostly in the form of ammonium (Simha *et al*., 2023). The TP content found was 17 mg/L, higher than that reported in the literature (Han *et al*., 2021) in the range of 4.3-5.5 mg/L. This is attributable to the high content of detergents and cleaning products, which contribute synthetic phosphates (Azam & Finneran, 2013). Nitrogen and phosphorus are considered pollutants that promote the eutrophication of water bodies, causing an imbalance in the ecosystem; however, in bioremediation systems using microalgae, these nutrients are consumed and tend to be the main precursors of cell growth and development (De Moraes *et al*., 2023).

Figure 3a shows the growth assays of *H. pluvialis* in MWW, where a similar cell density is observed at the beginning of the experiments in the 3 inoculum levels; however, statistically significant differences were found, indicating that a higher cell density was achieved with the 5% inoculum. The exponential growth phase was found to begin on day 10, where a deceleration in the increase of cell density is observed with the highest inocula (10% and 15%). The tendency of the lower inocula to reach higher cell concentrations is recurrent in wastewater bioremediation systems, as mentioned by Sales-Pérez *et al*. (2023b), where they used *N. oculata* for the treatment of poultry wastewater, varying the amount of inoculum at 3 levels (10%, 15%, and 20%), obtaining higher cell densities with the lower inoculum, while the higher inocula showed inhibition. This is generally attributed to the fact that in inocula with high volumes, nutrients (P, N, and C) are consumed quickly and with greater competition (Khalid *et al*., 2018). Another factor to consider is that in systems with high cell density, light access to the culture is reduced, mainly in the area of the photobioreactor walls, producing a self-shading effect inside, generating inefficient nutrient consumption and producing growth inhibition (Jeong & Jang, 2021).

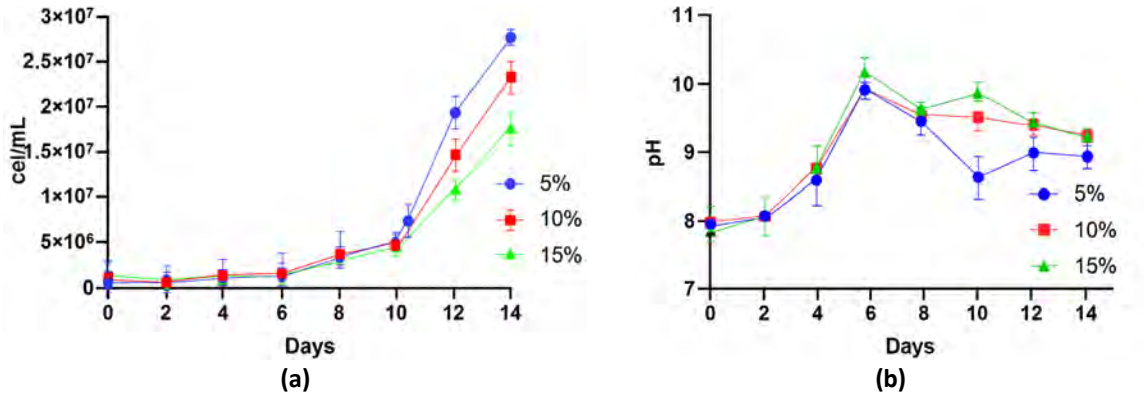

Figure 3. (a) Cell growth kinetics of *H. pluvialis* in MWW, (b) pH values determined during the growth of *H. pluvialis*.

Microalgae exhibit their highest growth rate in culture media with a pH between 7.0 and 8.4, a range in which bicarbonate (HCO_3^-) constitutes the predominant form of available inorganic carbon (Onyeaka *et al*., 2021). Figure 3b shows the variations in pH values during the experiment with the 3 inoculum levels. Similar behavior was found for all three inoculum levels, where from day 2 onwards there was an increase in pH until day 6. From that day until the end of the experiment, fluctuations between 10 and 8.5 were recorded. This tendency to alkalinize the medium is characteristic of microalgae systems and is directly related to the assimilation of carbon present in the wastewater by the microalgae. During the photosynthesis process within photobioreactors, microalgae rapidly fix CO2 in a reaction that initiates the Calvin-Benson cycle, ultimately producing carbohydrates (Amaro *et al*., 2023). This CO2 removal reaction shifts the carbonate system equilibrium, favoring the dissociation of bicarbonate (HCO_3^-) and carbonate (CO_3^{2-}), which generates hydroxyl ions and causes alkalinization of the medium, as shown in equations 5 and 6 (Abdel-Raouf *et al*., 2012).

$$2(HCO_3^-) \rightarrow CO_3^{2-} + H_2O + CO_2 \quad \textbf{(5)}$$

$$CO_3^{2-} + H_2O_2 \rightarrow 2OH^- + CO_2 \quad \textbf{(6)}$$

Microalgae treatments promoted the biodegradation of organic pollutants, converting them into simpler molecules and using the assimilated carbon for their growth and development (Zhou *et al*., 2022). Figure 4a shows the COD removals during the experiments with the 3 inoculum levels, which removed concentrations between 64-74% of COD, similar to those reported by Abdel-Raouf *et al*. (2012) who obtained 67% COD removals for biological systems in wastewater treatment using microalgae. In the removal of total COD, it is common to find a point in these types of systems where it no longer decreases; this may be due to a combination of several factors, such as the cell lysis process due to the stress caused by the aeration system, which causes the release of intracellular content, compensating for the preliminary COD reduction (Qiu *et al*., 2017). Furthermore, it should be mentioned that in the stationary phase of cell growth, an equilibrium is reached between the COD removal rate and the biomass generation rate (Sobolewska *et al*., 2024), which is organic matter susceptible to degradation, which may explain why no considerable COD reduction occurred after day 8. Regarding the statistical analysis, no significant differences were observed in tCOD removal among the three inoculum levels evaluated (one-way ANOVA, $p > 0.05$, $n = 4$). Post-hoc comparisons (Tukey's test) confirmed the absence of statistically significant pairwise differences. This lack of significant differences may be explained by the fact that tCOD includes both soluble and particulate organic fractions; while inoculum size can enhance the biodegradation of soluble organic matter, the particulate fraction tends to be less biodegradable and largely unaffected by inoculum concentration. Consequently, variations in inoculum percentage exerted only a minor influence on overall tCOD removal efficiency.

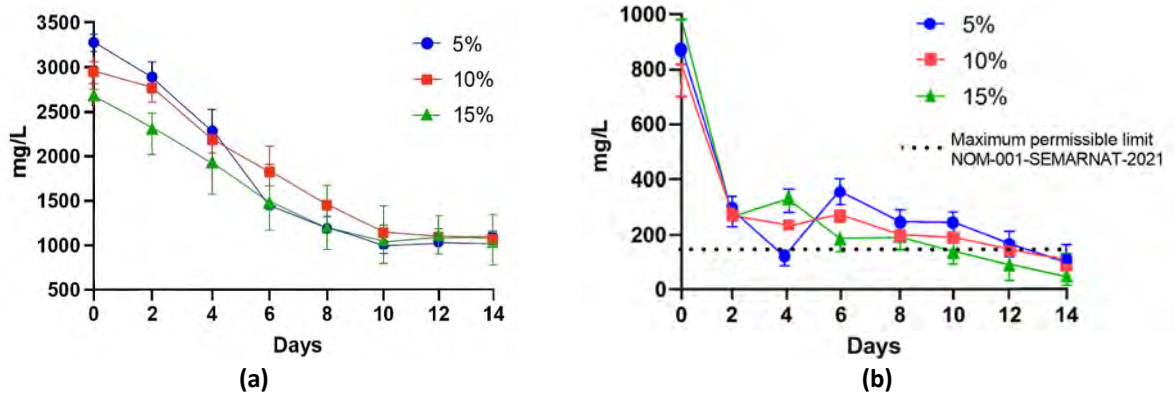

Figure 4. Behavior of the removal of (a) COD_T (b) COD_S.

Soluble COD (COD_s) is mainly composed of dissolved organic compounds and low molecular weight colloidal material (Płuciennik-Koropczuk & Myszograj, 2019). Figure 4b shows the removal of COD_S with the different inoculum concentrations evaluated, where a decreasing trend was observed from day 2 onwards, with removals of up to 70% for all experiments. Between days 2 and 10, fluctuating behavior was observed, with no significant changes in COD levels. Finally, after day 12, in all cases a decrease is observed until levels below the maximum permissible levels established in NOM-001-SEMARNAT-2021 (dotted line) are reached, obtaining a total removal of 92% - 99% for the 3 inoculum levels. However, statistically significant differences ($p < 0.05$, one-way ANOVA, $n = 4$) were observed among the inoculum percentages evaluated. Post-hoc analysis (Tukey's test) revealed that the highest COD_s removal percentages were obtained with 15%, which is consistent with the findings of Gentili (2014) who obtained a 92.7% removal of COD_s using Scenedesmus sp. in municipal wastewater combined with industrial wastewater. The decrease in COD in microalgae systems is caused by various factors, one of the main ones being the generation of EPS during microalgae metabolism. These compounds promote coagulation and the formation of flocs of colloidal particles; this new solid fraction is removed using mechanical operations such as centrifugation or sedimentation, thus reducing the COD concentration in the liquid phase (Xu *et al*., 2023).

Among the tested conditions, the 5% inoculum promoted the highest cell concentration, whereas the 15% inoculum achieved the greatest sCOD removal. However, only the 10% inoculum simultaneously ensured compliance with the regulatory discharge limits within the experimental timeframe in the shortest period, without exceeding biomass levels that could compromise reactor stability. Based on this predefined criterion, the 10% inoculum was selected for the scale-up experiments.

Figure 5a shows the results obtained in the airlift photobioreactor with *H. pluvialis* for the bioremediation of municipal wastewater; the green line shows cell growth and the blue line shows the decrease in COD_S over 14 days. The cell growth curve shows that the 0-6 day period was an adaptation phase; after that, a maximum concentration of 1.3 x 10^7 cells/mL was reached. Robles-Heredia *et al*. (2016) reported a similar maximum growth of 1.18 x 10^7 cells/mL of *Chlorella vulgaris* in an 11 L airlift photobioreactor. However, in this case, a lower cell concentration was obtained compared to experiments with 400 mL photobioreactors. This result is a common phenomenon when scaling up biological systems and can be explained by several interrelated factors affecting the availability of light, gases, and nutrients (Benner *et al*., 2022; Xu *et al*., 2009).

Figure 5a shows the behavior of COD_S during the 14 days of experimentation in the bioremediation system with the airlift-type photobioreactor. A significant decrease in COD_s was observed from day 2 until reaching values close to the maximum permissible limits from day 12, and by day 14 a maximum removal of 80% was achieved. This reduction can be explained by a series of synergistic mechanisms of a biological and physicochemical nature that operate simultaneously during the process. Firstly, during microalgal photosynthesis, CO_2 is used for biomass generation and the production of molecular oxygen (O_2). The O_2 acts as a terminal electron acceptor for heterotrophic bacteria that degrade dissolved organic compounds of low molecular weight such as volatile fatty acids, simple carbohydrates, and hydrosoluble proteins (Mathew *et al*., 2022). This is complemented by the secretion of EPS, which, as already mentioned, act as natural flocculants that also promote the coagulation of colloidal particles, that is, they transform the COD_S into a particulate fraction that is easily removed by sedimentation or filtration.

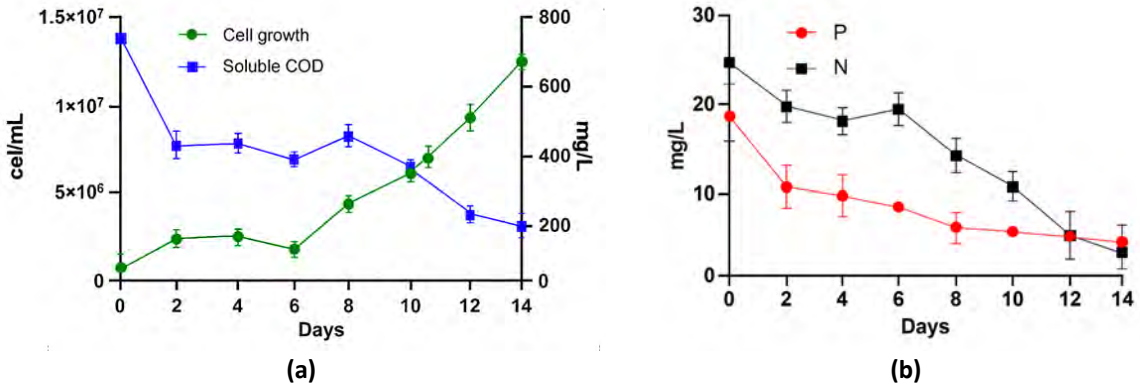

Figure 5. Behavior of the bioremediation process using *H. pluvialis* within the airlift FBR: (a) Removal of COD_S and cell growth; (b) Consumption of TP and TN.

The reduction of TP and TN in bioremediation systems represents a key component for the efficient treatment of wastewater, especially given the need to comply with environmental regulations in order to counteract eutrophication (Whitton *et al*., 2015). Figure 5b shows the decrease in concentration of TP (black line) and TN (red line), where removal percentages of 77% and 89% were obtained, respectively, both complying with the maximum permissible limits established by Mexican regulations (NOM-001-SEMARNAT-2021). It should be noted that this process was carried out under conditions characteristic of maintaining the vegetative phase of *H. pluvialis*, which favored the assimilation and consumption of these nutrients because, in this physiological phase, it has a high demand for nutrients to sustain the synthesis of essential biomolecules (Nahidian *et al*., 2018). In this study, the greatest reduction in phosphorus and nitrogen was observed during the active growth phase (between days 10-14), indicating that removal was mainly dominated by biological processes. Firstly, the nitrogen presents in the municipal wastewater in the form of ammonium (NH_4^+), nitrate (NO_3^-), and other organic forms, was incorporated by the microalgae for the synthesis of amino acids, proteins, nucleic acids, and pigments (Vega, 2018). On the other hand, phosphorus is absorbed as orthophosphate (PO_4^{3-}) and used in the formation of ATP, membrane phospholipids, and nucleic acids through phosphorylation (Su, 2020).

It has been demonstrated that the design of the photobioreactor directly influences the efficiency of bioremediation systems that use microalgae for wastewater treatment (Fu *et al*., 2019). The proposed design configuration and parameters allowed for continuous and smooth mixing, which prevented the presence of dead zones and cell shearing, and also promoted homogeneous distribution of light and nutrients. This increased the efficiency of the cultivation and

reaction conditions, allowing the processes of organic matter degradation, cell growth, and nutrient consumption to develop more efficiently, especially compared to static or poorly aerated systems.

In wastewater bioremediation systems that use microalgae, the incorporation of monitoring and control tools is fundamental to increasing process efficiency. In this context, rheology emerges as a valuable tool for evaluating the real-time state of the microalgal culture and its influence on the operation of the photobioreactor. This perspective is especially relevant in airlift-type photobioreactors, where the movement of the culture depends exclusively on the flow dynamics induced by aeration. Figure 6a shows the flow curves of the initial and final samples extracted from the photobioreactor during the bioremediation process. An increase in shear stress is observed in the final sample (blue line) compared to the initial sample due to the increase in biomass concentration during the photobioreactor's operation period. As the microalgae grew, a denser and more structured medium was generated. This higher cell concentration implies a greater resistance to flow, which translates into a higher shear stress, shifting from near-Newtonian to non-Newtonian behaviors.

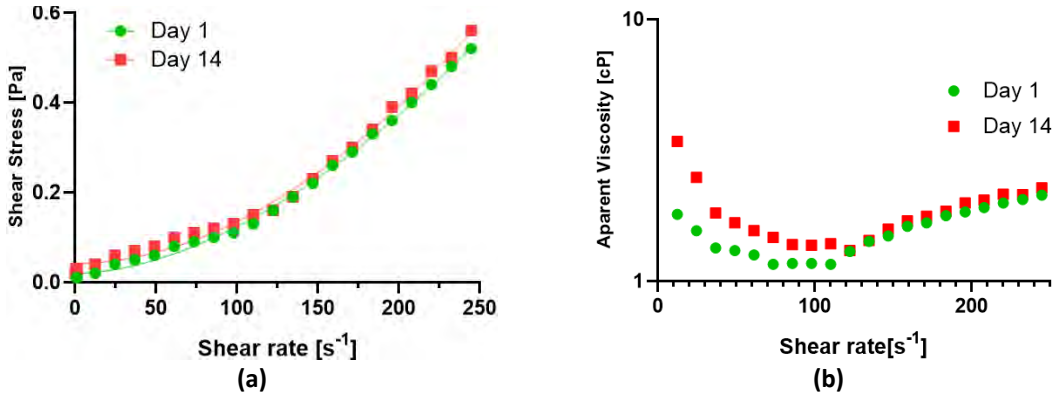

Figure 6. Initial and final rheological monitoring during the bioremediation process: (a) Rheogram (b) Apparent viscosities.

Figure 6b shows the apparent viscosity profiles of the initial and final samples from the microalgae treatment in the airlift photobioreactor. An increasing trend in apparent viscosity was observed in the final sample. It has been demonstrated that a moderate increase in apparent viscosity can be interpreted as a positive indicator of the process, as it evidences active growth, high cell productivity, and possible capture of dissolved organic matter in the liquid phase (Attar *et al*., 2023). This behavior, accompanied by initial, intermediate, and final variations in rheological parameters such as the consistency index (k) and the flow index (n) obtained from correlations with the models, allows the establishment of process control zones where the system is identified as having reached its maximum efficiency in both contaminant removal and biomass production. Similarly, the analysis of these parameters facilitates the determination of critical operating conditions that indicate the appropriate time to perform biomass extraction, thereby avoiding system saturation or losses in treatment efficiency.

The results of the rheological variables according to the commonly used models are shown in Table 2; the flow index n was greater than 1 in all the samples analyzed, therefore they were considered dilatant. In this case, the Herschel-Bulkley model had the correlation coefficient closest to unity, and therefore provided the best fit to the data. An increasing trend in the flow index n was observed during the sampling period, reaching a maximum value of 1.905 on day 14. This suggests that as microalgal biomass accumulates, these structures compact and reorganize under agitation, causing an increase in apparent viscosity at higher deformation rates. This behavior is similar to that reported by Gutiérrez-Casiano *et al*. (2022), who conducted a rheological monitoring of wastewater bioremediation from a poultry processing plant using *Chlorella vulgaris* in an airlift photobioreactor over 16 days. In the three samplings recorded (initial, intermediate, and final), the index n increased during the first 8 days of the process, which was related to the exponential phase of cell growth. In the last sampling, a slightly lower n value was recorded compared to the intermediate value, attributable to the decrease in cell-to-cell interactions and the generation of EPS due to the cell death phase. Therefore, an increase in n can be considered an indirect indicator of the accumulation of active biomass and the structural complexity of the system.

Table 2. Rheological parameters during the biodegradation process

Day	Model	τ_0	K	n	R^2
0	Ostwald de Waele	-	8.517e-005	1.583	0.9937
	Newton	-	0.001792	-	0.9356
	Herschel Bulkley	0.01985	3.186e-005	1.758	0.9974
2	Ostwald de Waele	-	8.831e-005	1.573	0.9918
	Newton	-	0.001754	-	0.9347
	Herschel Bulkley	0.02242	2.845e-005	1.773	0.9968
4	Ostwald de Waele	-	9.607e-005	1.554	0.9933
	Newton	-	0.001729	-	0.9388
	Herschel Bulkley	0.01907	3.725e-005	1.721	0.9970
6	Ostwald de Waele	-	9.657e-005	1.564	0.9884
	Newton	-	0.001834	-	0.9325
	Herschel Bulkley	0.02860	3.047e-005	1.764	0.9963
8	Ostwald de Waele	-	0.0001231	1.517	0.9871
	Newton	-	0.001828	-	0.9385
	Herschel Bulkley	0.02894	2.309e-005	1.818	0.9947
10	Ostwald de Waele	-	0.0002362	1.422	0.9736
	Newton	-	0.002139	-	0.9405
	Herschel Bulkley	0.04577	2.884e-005	1.758	0.9872
12	Ostwald de Waele	-	0.0001213	1.521	0.9817
	Newton	-	0.001839	-	0.9334
	Herschel Bulkley	0.03566	1.961e-005	1.844	0.9938
14	Ostwald de Waele	-	0.0001264	1.520	0.9792
	Newton	-	0.001905	-	0.9313
	Herschel Bulkley	0.04199	1.453e-005	1.905	0.9949

The correlation between the flow index (n) and cell density revealed a logarithmic relationship (equation 7), as shown in Figure 7a, with a determination coefficient of R^2 = 0.9182. This strong correlation suggests that the rheological behavior of the treated effluent within the reactor is closely associated with the development and accumulation of microalgal biomass. Specifically, the increase in cell density from 1.7×10^6 to 1.2×10^7 cells/mL resulted in a progressive rise in the flow index from 1.74 to 1.90. The logarithmic fit highlights that the greatest variations in the flow index occur at lower cell densities, whereas at higher concentrations the system tends to stabilize.

In a microalgae-based bioremediation system, a decrease in the consistency index (k) has been demonstrated to be a positive indicator of the removal of colloidal organic matter from wastewater (Schneider and Gerber, 2014). The consistency index remained constant in the range of $3 \times 10^{-5} – 2.3 \times 10^{-5}$ during the first 10 days of the process; however, from day 12 to day 14, it decreased to a value of 1.453×10^{-5}. These values can be related to the results obtained from the decrease in COD, since between days 2 and 10 the values fluctuated between 500 mg/L and 400 mg/L, until days 12 and 14, when a downward trend was observed. The behavior of this correlation is shown in Figure 7b, where the relationship between the consistency index (K) and the COD_s concentration exhibited a logarithmic fit (Equation 8) with a correlation coefficient of R^2 = 0.8144, indicating a consistent association between both variables. Nevertheless, the R^2 value lower than 0.9 suggests that the relationship is not fully explained by soluble COD concentration alone. This can be attributed to the fact that organic matter comprises both biodegradable and non-biodegradable compounds, the latter being metabolically unavailable but potentially contributing indirectly to the fluid viscosity. At the beginning of the process, the microalgal biomass primarily consumes biodegradable organic

compounds; however, as the process progresses, the degradation rate decreases due to the predominance of non-biodegradable organic matter and only a minor fraction of biodegradable compounds.

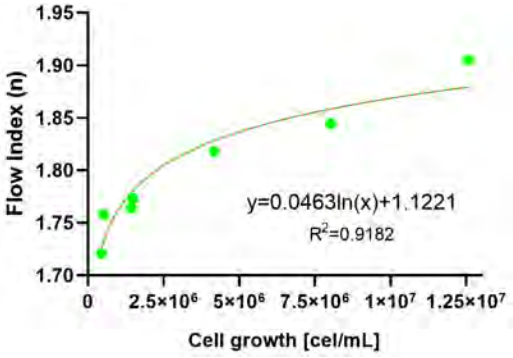

$$y = 0.0463\ ln\ (x) + 1.1221 \quad (7)$$

(a)

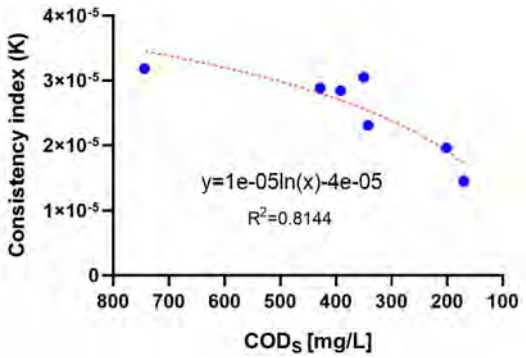

$$y = 1e - 05\ ln\ (x) - 4e - 05 \quad (8)$$

(b)

Figure 7. Correlation of (a) Flow index with cell density (b) Consistency index with CODs.

Conclusions

The MWW proved to be a suitable medium for the growth of *H. pluvialis*. Furthermore, adaptation tests showed that at low inoculum concentrations, inhibition phenomena caused by high substrate competition and self-shading are avoided. On the other hand, in the 400 mL photobioreactor experiments for the 3 inoculum levels evaluated, the organic matter content was effectively reduced, achieving removals greater than 64% of total COD and 92% of COD_S.

During the scale-up in the airlift photobioreactor, removals close to 80% of COD_S were obtained, and effective consumption of N and P was achieved, with both parameters remaining below the maximum permissible ranges according to Mexican regulations (NOM-001-SEMARNAT-2021). This confirms that the implementation of the airlift photobioreactor with the proposed configuration favored the optimal development of the culture, increasing the efficiency of pollutant removal and cell productivity.

The rheological monitoring carried out simultaneously with the kinetics of pollutant removal showed a dilatant behavior (n>1) characteristic of systems that use microalgae, and the affinity for fitting with the Herschel-Bulkley model allowed for establishing relationships of change with the rheological parameters of consistency index (k) and flow index (n). Monitoring these variables offers an indirect but robust approach to evaluate the physiological state of the culture, biomass accumulation, and the efficiency of soluble organic matter removal, which makes rheology a strategic control tool for the wastewater treatment process with the microalga *H. Pluvialis*.

Acknowledgments and Funding: The financial support granted by CONACYT through the scholarship with CVU 1323199.

Author contributions: U.C.-R.: writing, data collection, analysis and interpretation of data; J.M.M.-C.: editing, supervision, project administration and analysis of data; R.E.S.-P., J.E.-G., A.A.-L. and E.H.-A.: editing, conceptualization and data analysis.

References

Abdel-Raouf, N., Al-Homaidan, A., & Ibraheem, I. (2012). Microalgae and wastewater treatment. *Saudi Journal of Biological Sciences*, *19*(3), 257–275. https://doi.org/10.1016/j.sjbs.2012.04.005

Adesanya, V. O., Vadillo, D. C., & Mackley, M. R. (2012). The rheological characterization of algae suspensions for the production of biofuels. *Journal of Rheology*, *56*(4), 925–939. https://doi.org/10.1122/1.4717494

Amaro, H. M., Salgado, E. M., Nunes, O. C., Pires, J. C., & Esteves, A. F. (2023). Microalgae systems - environmental agents for wastewater treatment and further potential biomass valorisation. *Journal of Environmental Management*, *337*, 117678. https://doi.org/10.1016/j.jenvman.2023.117678

APHA, Wpcf, & AWWA. (2017). Standard methods for the examination of water and wastewater (23rd ed.). APHA.

Ata, R., Tore, G. Y., & Shah, M. P. (2021). Emerging technologies for treatment of antibiotic residues from wastewater influent/effluent for sustainable environment: A case study with NFC-doped titania immobilized on polystyrene as an efficient technology. *Current Research in Green and Sustainable Chemistry*, *4*, 100065. https://doi.org/10.1016/j.crgsc.2021.100065

Attar, S. B., Morillas-España, A., Sánchez-Zurano, A., Pessôa, L. C., Pinna-Hernández, M. G., De Jesus Assis, D., López, J. L. C., & Acién, G. (2023b). Influence of culture media composition on the rheology of microalgae concentrates on a large scale. New Biotechnology, 77, 90–99. https://doi.org/10.1016/j.nbt.2023.07.005

Azam, H. M., & Finneran, K. T. (2013). Fe(III) reduction-mediated phosphate removal as vivianite (Fe3(PO4)2·8H2O) in septic system wastewater. *Chemosphere*, *97*, 1–9. https://doi.org/10.1016/j.chemosphere.2013.09.032

Behin, J., & Amiri, P. (2023). A review of recent advances in airlift reactors technology with emphasis on environmental remediation. *Journal of Environmental Management*, *335*, 117560. https://doi.org/10.1016/j.jenvman.2023.117560

Bio6. (n.d.). https://rmiq.org/iqfvp/Pdfs/Vol.%2015,%20No.%202/Bio6/eBio6.html

Benner, P., Meier, L., Pfeffer, A., Krüger, K., Vargas, J. E. O., & Weuster-Botz, D. (2022). Lab-scale photobioreactor systems: principles, applications, and scalability. *Bioprocess and Biosystems Engineering*, *45*(5), 791–813. https://doi.org/10.1007/s00449-022-02711-1

De Moraes, L. B. S., Mota, G. C. P., Santos, E. P. D., Da Silva Campos, C. V. F., Da Silva, B. a. B., Gálvez, A. O., & De Souza Bezerra, R. (2023). Haematococcus pluvialis cultivation and astaxanthin production using different nitrogen sources with pulse feeding strategy. *Biomass Conversion and Biorefinery*, *14*(14), 16231–16243. https://doi.org/10.1007/s13399-023-03824-7

Estrada-García, J., Hernández-Aguilar, E., Romero-Mota, D. I., & Méndez-Contreras, J. M. (2023). Influence of anaerobic biotransformation process of agro-industrial waste with Lactobacillus acidophilus on the rheological parameters: case of study of pig manure. *Archives of Microbiology*, *205*(3). https://doi.org/10.1007/s00203-023-03437-8

Fu, J., Huang, Y., Liao, Q., Xia, A., Fu, Q., & Zhu, X. (2019). Photo-bioreactor design for microalgae: A review from the aspect of CO2 transfer and conversion. *Bioresource Technology*, *292*, 121947. https://doi.org/10.1016/j.biortech.2019.121947

Gutiérrez-Casiano, N., Hernández-Aguilar, E., Alvarado-Lassman, A., & Méndez-Contreras, J. M. (2022). Removal of carbon and nitrogen in wastewater from a poultry processing plant in a photobioreactor cultivated with the microalga Chlorella vulgaris. *Journal of Environmental Science and Health Part A*, *57*(7), 620–633. https://doi.org/10.1080/10934529.2022.2096986

Gutiérrez-Casiano, N., Hernández-Aguilar, E., Alvarado-Lassman, A., & Méndez-Contreras, J. M. (2022). Removal of carbon and nitrogen in wastewater from a poultry processing plant in a photobioreactor cultivated with the microalga Chlorella vulgaris. *Journal of Environmental Science and Health Part A*, *57*(7), 620–633. https://doi.org/10.1080/10934529.2022.2096986

Han, W., Jin, W., Li, Z., Wei, Y., He, Z., Chen, C., Qin, C., Chen, Y., Tu, R., & Zhou, X. (2021). Cultivation of microalgae for lipid production using municipal wastewater. *Process Safety and Environmental Protection*, *155*, 155–165. https://doi.org/10.1016/j.psep.2021.09.014 Huang, Y., Ragush, C. M., Johnston, L. H., Hall, M. W., Beiko, R. G., Jamieson, R. C., & Hansen, L. T. (2021). Changes in bacterial communities during treatment of municipal wastewater in arctic wastewater stabilization ponds. Frontiers in Water, 3. https://doi.org/10.3389/frwa.2021.710853

Jeong, D., & Jang, A. (2021). Mitigation of self-shading effect in embedded optical fiber in Chlorella sorokiniana immobilized polyvinyl alcohol gel beads. *Chemosphere*, *283*, 131195. https://doi.org/10.1016/j.chemosphere.2021.131195

Khalid, A. a. H., Yaakob, Z., Abdullah, S. R. S., & Takriff, M. S. (2018). Analysis of the elemental composition and uptake mechanism of Chlorella sorokiniana for nutrient removal in agricultural wastewater under optimized response surface methodology (RSM) conditions. *Journal of Cleaner Production*, *210*, 673–686. https://doi.org/10.1016/j.jclepro.2018.11.095

Laroche, C. (2022). Exopolysaccharides from Microalgae and Cyanobacteria: Diversity of Strains, Production Strategies, and Applications. *Marine Drugs*, *20*(5), 336. https://doi.org/10.3390/md20050336

Li, L., Xu, X., Wang, W., Lau, R., & Wang, C. (2022). Hydrodynamics and mass transfer of concentric-tube internal loop airlift reactors: A review. *Bioresource Technology*, *359*, 127451. https://doi.org/10.1016/j.biortech.2022.127451

Mathew, M. M., Khatana, K., Vats, V., Dhanker, R., Kumar, R., Dahms, H., & Hwang, J. (2022). Biological Approaches Integrating Algae and Bacteria for the Degradation of Wastewater Contaminants—A Review. *Frontiers in Microbiology*, *12*. https://doi.org/10.3389/fmicb.2021.801051

Mazziero, V. T., Batista, V. G., De Oliveira, D. G., Scontri, M., De Paula, A. V., & Cerri, M. O. (2022). Characterization of packed-bed in the downcomer of a concentric internal-loop airlift bioreactor. *Biochemical Engineering Journal*, *181*, 108407. https://doi.org/10.1016/j.bej.2022.108407

Nahidian, B., Ghanati, F., Shahbazi, M., & Soltani, N. (2018). Effect of nutrients on the growth and physiological features of newly isolated Haematococcus pluvialis TMU1. *Bioresource Technology*, *255*, 229–237. https://doi.org/10.1016/j.biortech.2018.01.130

Onyeaka, H., Miri, T., Obileke, K., Hart, A., Anumudu, C., & Al-Sharify, Z. T. (2021). Minimizing carbon footprint via microalgae as a biological capture. *Carbon Capture Science & Technology*, *1*, 100007. https://doi.org/10.1016/j.ccst.2021.100007

Pan, M., Zhu, X., Pan, G., & Angelidak, I. (2021). Integrated valorization system for simultaneous high strength organic wastewater treatment and astaxanthin production from Haematococcus pluvialis. *Bioresource Technology*, *326*, 124761. https://doi.org/10.1016/j.biortech.2021.124761

Pérez-Guzmán, S. M., Hernández-Aguilar, E., Rosas-Mendoza, E. S., Alvarado-Lassman, A., & Méndez-Contreras, J. M. (2024). Efecto de la presión de saturación en la operación en modo batch de un reactor DAF escala laboratorio para el tratamiento de efluentes municipales. *Tendencias en Energías Renovables y Sustentabilidad* ., *3*(1), 139–144. https://doi.org/10.56845/terys.v3i1.218

Płuciennik-Koropczuk, E., & Myszograj, S. (2019). New approach in COD fractionation methods. *Water*, *11*(7), 1484. https://doi.org/10.3390/w11071484

Qiu, R., Gao, S., Lopez, P. A., & Ogden, K. L. (2017). Effects of pH on cell growth, lipid production and CO2 addition of microalgae Chlorella sorokiniana. *Algal Research*, *28*, 192–199. https://doi.org/10.1016/j.algal.2017.11.004

Radice, R. P., Grassi, G., Capasso, G., Montagnuolo, E., Aiello, D., Perna, A. M., Marzocco, S., & Martelli, G. (2024). Five mutated genotypes of Haematococcus pluvialis useful for crude oil wastewater bioremediation. *Algal Research*, *83*, 103693. https://doi.org/10.1016/j.algal.2024.103693

Robles-Heredia, J. C., Sacramento-Rivero, J. C., Ruiz-Marín, A., Baz-Rodríguez, S., Canedo-López, Y., & Narváez-García, A. (2016). Evaluation of cell growth, nitrogen removal and lipid production by chlorella vulgaris to different conditions of aeration in two types of annular photobioreactors. *Revista Mexicana De Ingeniería Química*, *15*(2), 361–377.

Rout, P. R., Shahid, M. K., Dash, R. R., Bhunia, P., Liu, D., Varjani, S., Zhang, T. C., & Surampalli, R. Y. (2021). Nutrient removal from domestic wastewater: A comprehensive review on conventional and advanced technologies. *Journal of Environmental Management*, *296*, 113246. https://doi.org/10.1016/j.jenvman.2021.113246

Sales-Pérez, R. E., Sales-Chávez, R. M., Romero-Mota, D. I., Estrada-García, J., & Méndez-Contreras, J. M. (2023a). Removal of organic matter during adaptation of Nannochloropsis oculata in livestock waste. *Renewable Energy Biomass & Sustainability*, *5*(2), 32–39. https://doi.org/10.56845/rebs.v5i2.93

Schneider, N., & Gerber, M. (2014). Correlation between viscosity, temperature and total solid content of algal biomass. *Bioresource Technology*, 170, 293–302. https://doi.org/10.1016/j.biortech.2014.07.107

Simha, P., Vasiljev, A., Randall, D. G., & Vinnerås, B. (2023). Factors influencing the recovery of organic nitrogen from fresh human urine dosed with organic/inorganic acids and concentrated by evaporation in ambient conditions. *The Science of the Total Environment*, *879*, 163053. https://doi.org/10.1016/j.scitotenv.2023.163053

Singh, V., Phuleria, H. C., & Chandel, M. K. (2017). Greenhouse Gas Emissions from Sewage Treatment Plants Based on Sequential Batch Reactor in Maharashtra. In Water science and technology library. In V. Singh, S. Yadav, & R. Yadava (Eds.), *Climate change impacts* (pp. 195–210). Springer.https://doi.org/10.1007/978-981-10-5714-4_13

Sobolewska, E., Borowski, S., & Nowicka-Krawczyk, P. (2024). Cultivation of microalgae in liquid digestate to remove nutrients and organic contaminants. *BioEnergy Research*, *17*(3), 1843–1855. https://doi.org/10.1007/s12155-024-10753-4

Su, Y. (2020). Revisiting carbon, nitrogen, and phosphorus metabolisms in microalgae for wastewater treatment. *The Science of the Total Environment*, *762*, 144590. https://doi.org/10.1016/j.scitotenv.2020.144590

Tang, J., Qu, X., Chen, S., Pu, Y., He, X., Zhou, Z., Wang, H., Jin, N., Huang, J., Shah, F., Hu, Y., & Abomohra, A. (2023). Microalgae cultivation using municipal wastewater and anaerobic membrane effluent: lipid production and nutrient removal. *Water*, *15*(13), 2388. https://doi.org/10.3390/w15132388

Uyar, B., Ali, M. D., & Uyar, G. E. O. (2024). Design parameters comparison of bubble column, airlift and stirred tank photobioreactors for microalgae production. *Bioprocess and Biosystems Engineering*, *47*(2), 195–209. https://doi.org/10.1007/s00449-023-02952-8

Vega, J. M. (2018). Nitrogen and sulfur metabolism in microalgae and plants: 50 years of research. In F. Cánovas, U. Lüttge, C. Leuschner, & M. C. Risueño (Eds.), *Progress in botany* (Vol. 81, pp. 143–169). Springer. https://doi.org/10.1007/124_2018_26

Wang, H., Qi, B., Jiang, X., Jiang, Y., Yang, H., Xiao, Y., Jiang, N., Deng, L., & Wang, W. (2019). Microalgal interstrains differences in algal-bacterial biofloc formation during liquid digestate treatment. *Bioresource Technology*, *289*, 121741. https://doi.org/10.1016/j.biortech.2019.121741

Whitton, R., Ometto, F., Pidou, M., Jarvis, P., Villa, R., & Jefferson, B. (2015). Microalgae for municipal wastewater nutrient remediation: mechanisms, reactors and outlook for tertiary treatment. *Environmental Technology Reviews*, *4*(1), 133–148. https://doi.org/10.1080/21622515.2015.1105308

Wu, Z., Duan, H., Li, K., & Ye, L. (2022). A comprehensive carbon footprint analysis of different wastewater treatment plant configurations. *Environmental Research*, *214*, 113818. https://doi.org/10.1016/j.envres.2022.113818

Xu, H., Tang, Z., Yang, D., Dai, X., & Chen, H. (2023). Enhanced growth and auto-flocculation of Scenedesmus quadricauda in anaerobic digestate using high light intensity and nanosilica: A biomineralization-inspired strategy. *Water Research*, *235*, 119893. https://doi.org/10.1016/j.watres.2023.119893

Xu, L., Weathers, P. J., Xiong, X., & Liu, C. (2009). Microalgal bioreactors: Challenges and opportunities. *Engineering in Life Sciences*, *9*(3), 178–189. https://doi.org/10.1002/elsc.200800111

Zhang, W., Yong, Y., Zhang, G., Yang, C., & Mao, Z. (2014). Mixing Characteristics and Bubble Behavior in an Airlift Internal Loop Reactor with Low Aspect Ratio. *Chinese Journal of Chemical Engineering*, *22*(6), 611–621. https://doi.org/10.1016/s1004-9541(14)60089-6

Zhou, J., Yang, L., Huang, K., Chen, D., & Gao, F. (2022). Mechanisms and application of microalgae on removing emerging contaminants from wastewater: A review. *Bioresource Technology*, *364*, 128049. https://doi.org/10.1016/j.biortech.2022.128049

Cost analysis and manufacturing process of blade prototypes with different structural configurations for a 1 kW H-type vertical axis wind turbine

Giovanni Vidal-Flores *, Farid Quijada-Escamilla, Jose Rafael Gomez-Bautista, Isaías Alvarado-Medrano

Gerencia de Energía, Centro de Tecnología Avanzada (CIATEQ), El Marqués, Querétaro, México
* Corresponding author: giovanni.vidal@ciateq.mx

Received: November 1, 2024 Accepted: October 6, 2025 Published: November 27, 2025
DOI: https://doi.org/10.56845/rebs.v7i2.643

Abstract: This article analyzes the costs associated with the manufacturing processes of prototype blades, each measuring 2 meters in length and featuring a NACA 0015 aerodynamic profile, with different structural configurations for a 1 kW H-type vertical axis wind turbine (VAWT). The research identifies the material costs and mass of the blades in order to optimize their manufacturing and achieve efficient performance. The objective is to improve resource efficiency in both research and industrial processes. Two manufacturing methods are evaluated: hand lay-up molding (Prototype A) and vacuum-assisted resin transfer molding (VARTM, Prototypes B and C). The evaluation criteria included manufacturing cost, weight, and quality. Prototype A, a single-piece blade with an EPS core, showed the lowest mass (5.11 kg) and cost, though it required significant surface repairs due to resin slippage, which could affect aerodynamic performance. Prototypes B and C, produced by VARTM with a double-shell design, achieved superior surface quality and a controlled fiber-to-resin ratio (100:50). Prototype B weighed 5.81 kg, while Prototype C, reinforced with a polyurethane core for greater rigidity, was the heaviest at 7.22 kg. However, their manufacturing costs were considerably higher: 215% (B) and 312% (C) compared to Prototype A, mainly due to the use of specialized materials. The results highlight the trade-offs between cost, mass, and quality, offering a reference for the development of structurally efficient and economically viable VAWT blades for urban applications. The conclusions are especially relevant for guiding future design and manufacturing decisions for VAWTs intended to operate in challenging environments characterized by turbulent and low-speed winds.

Keywords: VAWT, composite materials enhancement, VARTM procedure, blade manufacture, cost analysis.

Introduction

Wind energy is one of the most important sources of renewable energy worldwide. The two primary configurations of wind turbines used to harness wind energy are Vertical Axis Wind Turbines (VAWTs) and Horizontal Axis Wind Turbines (HAWTs). Each configuration has its own advantages and disadvantages. The main advantages of VAWTs over HAWTs include their omnidirectionality—allowing them to capture wind from any direction—as well as their suitability for lower wind speeds and urban environments. In addition, VAWTs offer a more compact design, generate lower noise levels, and are generally easier to maintain. On the other hand, the design of VAWTs can result in higher structural stress and significant torque fluctuations, which may affect their reliability and lifespan. Nevertheless, continued investment in VAWT technology has the potential to drive innovations that enhance efficiency, durability, and cost-effectiveness while reducing environmental impact. Such advancements could open new markets and complement existing wind technologies, ultimately contributing to a more diverse and resilient renewable energy landscape.

Since the development of the Savonius and Darrieus types of VAWTs in the 1930s, several alternative designs have emerged in pursuit of higher efficiency, including the H-rotor and the helicoidal rotor. The first wave of experimental research, prototype testing, and commercial models took place during the 1980s and 1990s, with the introduction of the Φ-type VAWT rotor. By 2010, commercial H-type VAWT rotors were deployed for small-scale electricity generation (Stoevesandt *et al.*, 2020). In recent years, renewed interest in VAWTs has emerged, with two major applications being identified: advancements in offshore installations and the development of small-scale VAWTs designed for highly turbulent environments, such as urban areas.

The new interest in VAWT technology is towards offshore applications due to the great wind potential at sea, allowing the development of this type of technology on a large scale and taking as a reference the offshore wind energy installation prospects in Europe for 2023-2027 with a capacity of 129 GW (Brandetti, 2024). Some research has been conducted on the challenges due to the harsh environment, as well as on the analysis of experimental prototypes (Ghigo *et al.*, 2024), studies on the design of floating offshore wind turbine platforms (Edwards *et al.*, 2024), innovative design of a lightweight modular floating foundation for offshore VAWTs to reduce operating costs (Boo *et al.*, 2023),

and on the development of numerical design and analysis tools to ensure engineering for aero-hydro-servo-elastic simulations of VAWT (Devin, 2023).

With the new challenges to mitigate energy deficiency in areas with little infrastructure and even for the development of "smart cities" or the implementation of smart grids, the development of smart wind farms with VAWT has been chosen, specifically in areas where there is a low wind speed or high turbulence. Nowadays, several commercial models of VAWT are marketed, manufacturing components (such as blades) with some conventional materials such as aluminum and composite materials, both with advantages and disadvantages according to the operation conditions.

VAWT applications in turbulent environments such as urban and rural areas have great potential on a large-scale to supply power to buildings, street lighting or to store energy for use in other small applications. Additionally, some research has been developed to improve current technology. These research include the development of a design methodology to understand the effect of geometrical parameters in the performance of VAWT (Cuevas-Carvajal *et al.*, 2022), improving the aerodynamic efficiency of VAWT with numerical simulations of new blade designs without an expensive manufacturing process (Mendoza and Bernhoff, 2020), a proposals of roof top building modifications based on CFD analysis for the installation of VAWTs to increase wind energy harvesting in urban areas (Juan *et al.*, 2024), structural optimization of H-type VAWT rotor to reduce blade mass and avoid peak stresses and strain limits (Marzec *et al.*, 2023) and optimizing efficiency using fixed deflector fins by reducing production materials and maximizing annual energy production (AEP) (Marinić-Kragić *et al.*, 2022), including algorithms that define an optimal structural design of the blade with the parameters of laminate thickness, reinforcement orientation, Fiber-to-Volume Fraction (FvF), resin matrix and number of reinforcement layers (Geneid *et al,*. 2022).

Efforts have been made to optimize aerodynamic performance, develop new prototypes, optimize costs, develop simulation tools, and develop new design and manufacturing methodologies to achieve new applications with VAWT technologies. In this work, an analysis is shown to find a balance between material costs and low mass criteria for a VAWT that could take advantage of low speeds with good long-term performance. The aim is to save resources in manufacturing processes at the research and industrial level.

Furthermore, this report serves as a model for those developers such as research centers, academia, small industry, and independent developers who in their work carry out manufacturing processes of small wind turbines, in such a way that they can take it as a reference to delve into the cost. The long-term goal is to replicate a final design for urban applications with high turbulence environments and low wind speeds, ensuring a good structural design of VAWT blades with a service life in accordance with the IEC 61400-2: Small wind turbines (IEC, 2013).

Materials and Methods

I. Background

Composite materials

Composite materials are formed by combining two or more constituent elements, primarily a matrix and a reinforcement, to enhance their mechanical properties. The most common hand-made composite materials are Polymer Matrix Composites (PMCs), Metal Matrix Composites (MMCs), and Ceramic Matrix Composites (CMCs). These materials can be tailored to achieve specific mechanical properties by carefully selecting their constituents, proportions, distribution, structural arrangement, interfacial composition, and other factors (Chawla, 2019).

The reinforcement is typically in fiber form, being the most common glass fiber; Its primary function is to support loads along the longitudinal direction while providing minimal strength in the transverse direction. Structural reinforcements are **E – glass (electrical)**, **C – glass (chemical)** and **R, S or T – glass (ballistic applications)** (Gurit, 2016). Other forms include carbon, aramid, ceramics, boron, polyester or natural fibers (Chawla, 2019).

The matrix in composite materials can take various forms, including epoxy, polyester, and vinylester. These matrices, commonly referred to as polymers, consist of long chain-like molecules made up of repeated units, often called synthetic resins or simply resins. Resins are generally classified into two types: **thermoplastics**, which undergo a

reversible process (e.g., nylon, ABS, polypropylene), and **thermosets**, which undergo a non-reversible process (e.g., epoxy, polyester) (Gurit, 2016).

Applied loads and stresses are primarily transmitted along the reinforcements, while the matrix protects the reinforcements from environmental degradation and maintains their position within the composite structure (see Figure 1) (Alvarado, 2023).

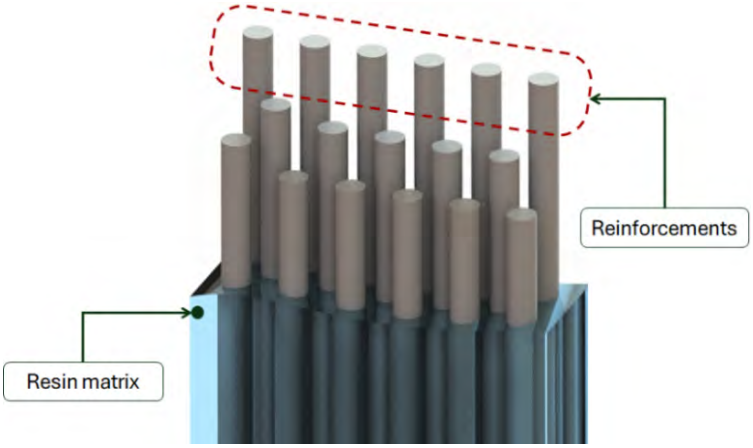

Figure 1. Schematic representation of the general composition of a composite material (matrix and reinforcements).

The Fiber Volume Fraction (FvF) is defined as the ratio of the total volume of reinforcements to the overall volume of the composite material. This parameter is important because it influences the strength and stiffness of the composite and depends on the reinforcement structure (e.g., type of weave) as well as the manufacturing process.

Glass fiber reinforcements in wind industry

For wind energy industry applications, the most widely used are continuous fibers. These reinforcements have a commercial presentation in the form of a ply, where these reinforcements are woven to create a ply with a specific orientation according to application requirements. Typical orientations are shown in Figure 2:

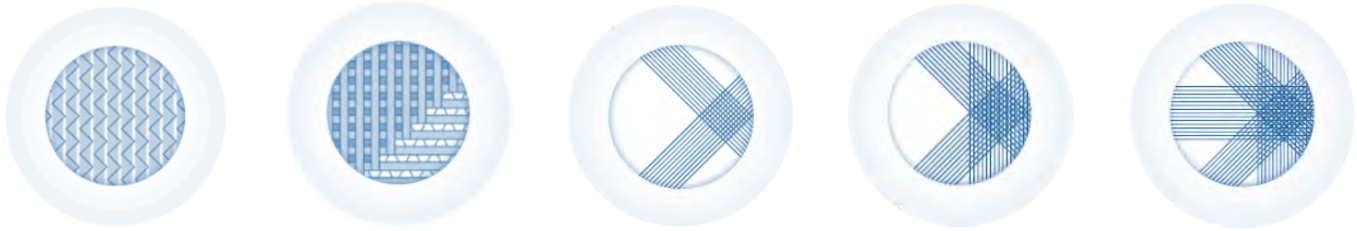

Figure 2. Typical orientation of continuous fiber reinforcements (Gurit, 2016).

Resin Matrix in wind industry

Thermoset epoxy resins are widely used in the wind industry, in the manufacturing and repairing processes for wind turbine blades, thanks to their excellent manufacturing flexibility and mechanical properties (KUKDO, 2011).

II. Process definition

Several production processes exist in wind industry to obtain the final product. These processes can be classified into open molding and closed molding as shown in the Table 1:

Table 1. Manufacturing methods with composite materials (Lee *et al.*, 2021).

Open molding	Closed molding
• Hand lay-up • Filament winding • Spray up	• Pre-preg • Resin transfer molding (RTM) • Vacuum infusion • Compression molding • Pultrusion

The Wind Energy Innovation Laboratory at CIATEQ has the infrastructure to carry out two types of manufacturing processes with composite materials: the hand lay-up and the Vacuum Assisted Resin Transfer Molding (VARTM). The VARTM process is widely employed in the production of wind turbine blades, ranging from small to large scales.

Hand lay-up process

In this process, the resin is manually poured over the fiberglass layers and then distributed across the entire surface using impregnation rollers. This process is among the most cost-effective in the industry, as it requires relatively few consumables, tools or specialized equipment, and the primary materials are inexpensive. However, achieving proper lamination requires skill to ensure uniform fiber impregnation and to avoid excessive application of the resin matrix.

VARTM process

This process requires a mold with the shape of the component and consumables as depicted in Figure 3. The general steps of this process are as follows:

Step 1: Prepare the mold surface (1) before applying the fiberglass layers with release film, then place the tacky-tape (2) over the perimeter on the mold surface.
Step 2: Stack the fiberglass layers (3) according to the laminate drawings.
Step 3: Place the consumables on the laminate according to the infusion diagrams; peel-ply (4), runner (5), inlet and outlet hose (6,7).
Step 4: Tape the vacuum-bag (8) with the tacky-tape (2), make sure there are no gaps that allow air to enter.
Step 5: Connect the outlet hose (7) with the vacuum pump (9,10) to extract the air from inside the vacuum-bag (8) by compacting the stacked fiberglass layers (3).
Step 6: Perform a vacuum test before allowing the entry of epoxy resin.
Step 7: Mix the epoxy resin (11) and connect directly to the inlet hose.
Step 8: Control the process infusion (12) until all the fiberglass layers are completely impregnated.
Step 9: Control the temperature for the curing process
Step 10: Demolding, trimming, dimensional control and painting process.

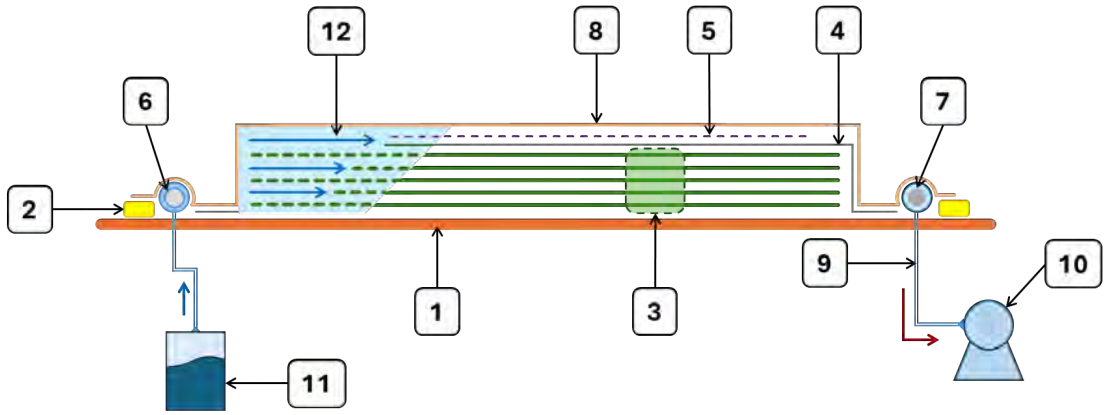

Figure 3. Elements of a VARTM process.

III. Experimental Set-up

The experimental configuration for this work was designed to compare the costs associated with two manufacturing methods for the fabrication of a blade model (see Table 2 for characteristics of the VAWT blade): Hand lay-up process (Prototype A) and VARTM process. The VARTM method was further evaluated in two variants: Prototype B (without shear web) and Prototype C (with shear web). The evaluation criteria considered included manufacturing cost, weight and quality associated to each process. According to a previous study, weight is an important factor in achieving a low starting torque at low wind speeds for the design of a 1 kW VAWT (Vidal-Flores y Hernández-Arriaga, 2024).

Prototypes A, B, and C utilize continuous E-glass fiber reinforcements oriented in unidirectional (0°) and biangular (+45°/-45°) configurations. The reinforcement fibers were supplied by SAERTEX, a commercial brand providing materials for wind energy applications in Mexico. The resin matrix was supplied by KUKDO CHEMICAL HQ. The details of the manufacturing process are described in the following sections.

Table 2. General characteristics of the VAWT blade.

Characteristic	Data
Blade span	2 m
Airfoil	NACA 0015
Chord	20 cm
Materials	Fiberglass, epoxy resin and structural adhesive, cores and coating.

Prototype A – Hand Lay-Up Manufacturing Process

The manufacturing method for Prototype A involves using an expanded polystyrene (EPS) core covered with a biaxial fiberglass (BX-FG) layer impregnated with epoxy resin, as illustrated in Figure 4. This process results in the fabrication of a single-piece VAWT blade.

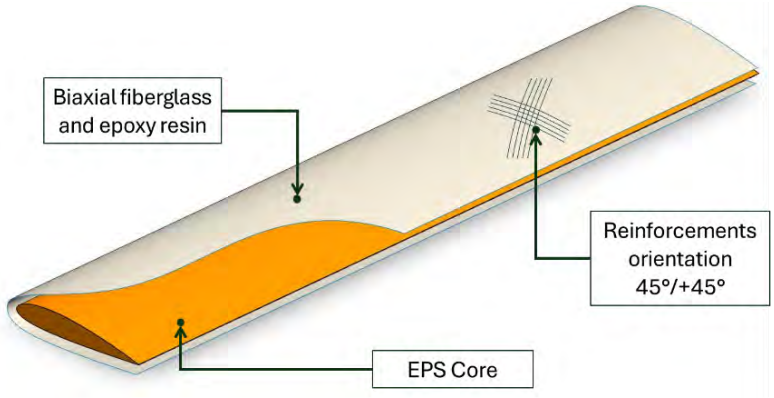

Figure 4. Structural design of Prototype A.

The hand lay-up manufacturing process for prototype A is described as follows:

A-1) Prototype A – Core Preparation (EPS Material)
A piece of EPS, corresponding to the full blade length (2 m), is shaped using wooden templates representing the NACA 0015 airfoil profile at each cross-section. Lateral wooden panels are also attached to form a bolted frame, as illustrated in Figure 5-(a). The EPS core is then cut using a hot wire guided by the wooden profiles on both the upper and lower sides, resulting in a finished EPS core with a total mass of 1.1 kg.

A-2) Prototype A – Laminate Application
The EPS core is covered with biaxial fiberglass (BX-FG) oriented longitudinally to ensure proper epoxy resin impregnation and uniform adhesion of the fibers across the entire surface of the core, as illustrated in Figure 5-(b).

(a) **(b)**

Figure 5. (a) Wood guides for EPS core, and (b) Biaxial fiberglass on EPS core.

The mass of the BX-FG before resin impregnation is 0.71 kg, calculated as the product of the layer's area density and total surface area, as shown in Equation 1. An additional 3 cm is added to the width of the BX-FG layer to ensure complete coverage of the EPS core. The biaxial fiberglass (BX-FG) has a standard surface density of 830 g/m², according to the manufacturer SAERTEX.

$$m_{BD-FG} = (0.83kg\ /\ m^2\ )(2\ m)(0.43\ m) = 0.71\ kg \quad \textbf{(1)}$$

In a manual lamination process, an additional percentage of epoxy resin must be considered, as this method provides less control over resin impregnation and the fiber volume fraction (FvF).

Prototype A – Epoxy resin impregnation and curing

A-3) The total epoxy resin matrix used for Prototype A is 1.2 kg, including an allowance for excess. After manual impregnation, the prototype is placed in a curing oven. This curing process, conducted at a constant temperature of 80 °C for 10 hours, ensures optimal mechanical properties of the composite. The curing parameters follow the recommendations of the resin manufacturer, KUKDO CHEMICAL HQ (KUKDO, 2011).

Prototype A – Surface finishing

A-4) Once the curing procedure is done, the surface imperfections must be examined, considering a repairing process on the surface of prototype A due to the sliding of the epoxy resin matrix by the effects of gravity. A rough surface is obtained by the fiberglass filaments, which affects the aerodynamic performance (Bai et al., 2014).

For the repairing process, a layer of epoxy filler is applied to the surface, which must cover the defects without modifying the aerodynamic surface. The total mass of the epoxy filler for prototype A is 1.45 kg.

A-5) To protect the composite from degradation by solar radiation a coating is necessary, the painting process uses a polyurethane paint. The total coating mass is 0.65 kg, which is applied with a paint spray gun. The list of materials for prototype A is shown in Table 3.

Table 3. List of materials for prototype *A*

Material	**Commercial data**
BX-FG	SAERTEX X-E-830 gsm (SAERTEX, 2022)
Epoxy resin matrix	KUKDO epoxy systems (KUKDO, 2011)
EPS core	FANOSA EPS
Epoxy filler	-
Coating	Polyurethane paint COMEX (COMEX, 2024)

Prototype B – VARTM Manufacturing Process

In Prototype B, the blade is composed of two separate parts: an upper shell (shell 1) and a lower shell (shell 2), which are bonded together using an epoxy structural adhesive. Unidirectional fiberglass (UD-FG) with an area density of 1180 g/m² and biaxial fiberglass (BX-FG) with an area density of 830 g/m², both supplied by SAERTEX, were used in the design of this prototype (see Figure 6).

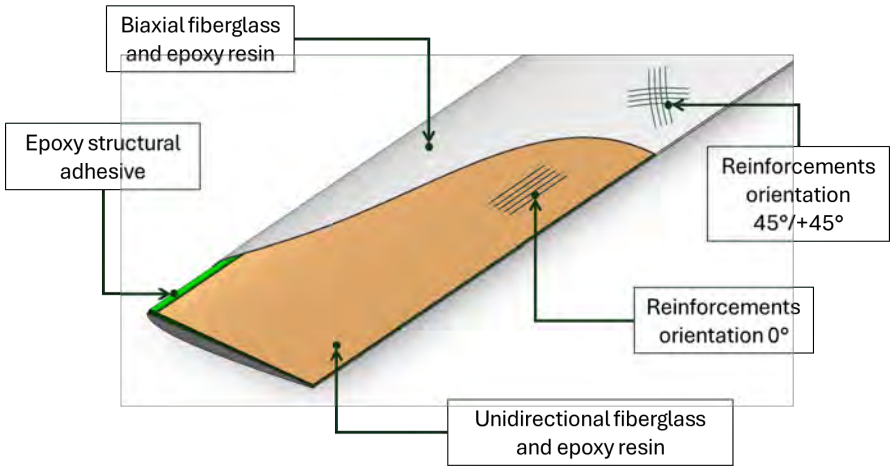

Figure 6. Structural design of prototype B.

Prototype B – Mold preparation

B-1) For the manufacture of Prototypes B, a master plug and mold were created. The master plug was fabricated from MDF sheets, which were bonded with glue to form an MDF block. This block was then machined using a CNC machine to produce the surface profile of the blade, see Figure 7-(a). The mold was subsequently created from the master plug, see Figure 7-(b).

(a) **(b)**

Figure 7. (a) Master plug machined with CNC machine, and (b) Mold for 1 kW VAWT blade.

B-2) The structural lamination for prototypes B consists of 4 layers of fiberglass per shell, with careful control of the filament orientation in each layer. Lamination begins with three layers of biaxial fiberglass (BX-FG), followed by a final layer of unidirectional fiberglass (UD-FG) placed directly on the mold surface, as illustrated in Figure 8.

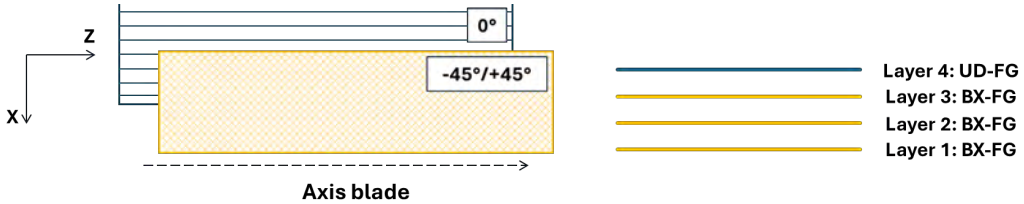

Figure 8. Reference alignment system for fiberglass layer lamination.

The total mass of the dry fiberglass layers is 1.55 kg for each shell. The mass of a single BX-FG layer is 0.35 kg, while the UD-FG layer has a mass of 0.5 kg.

Prototype B – VARTM process Set-up

B-3) After stacking the fiberglass layers, the consumables required for the VARTM process are positioned, as shown in Figure 9-(a). Based on a fiber volume fraction (FvF) of 100:50 for the infusion process, the total mass of the epoxy resin matrix is 0.78 kg per shell. During resin infusion, any vacuum-bag leaks should be checked and minimized before allowing the epoxy resin to enter the mold, see Figure 9-(b).

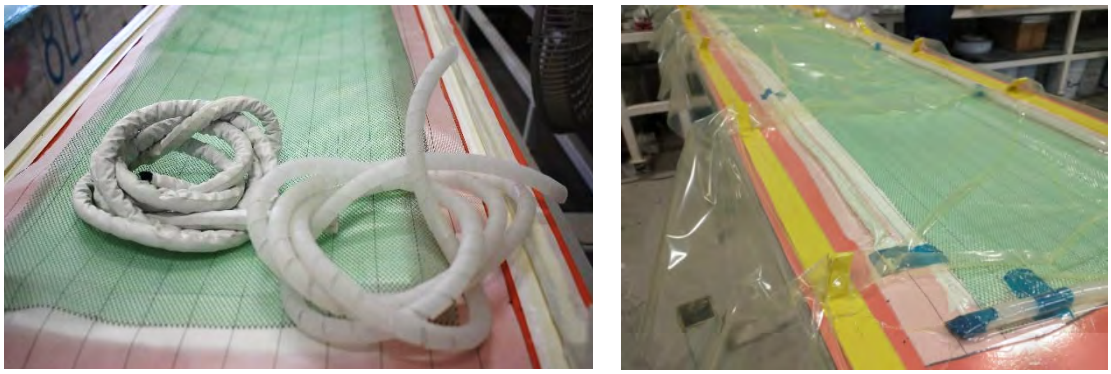

(a) **(b)**

Figure 9. (a) Consumables for the VARTM process, and (b) Vacuum-bag leakage inspection.

B-4) After the resin infusion is complete, each shell is placed in an oven for curing at 80 °C for 10 hours. Once the shells are fully cured, the consumables are removed in preparation for the trimming process, see Figure 10.

Figure 10. Inspection of the surface of the shell prototype B.

B-5) A bond line of epoxy structural adhesive, with a total mass of 0.5 kg, is applied along the inner perimeter of Shell 1. Shell 2 is then placed over Shell 1, carefully aligning the leading and trailing edges, and uniform pressure is applied across the entire surface to ensure proper bonding. Similar to the curing of the epoxy resin matrix, the epoxy structural adhesive undergoes a curing process in an oven at 80 °C for 10 hours.

B-6) During the bonding process, some epoxy structural adhesive bled around the blade. This excess material must be carefully removed without altering the blade geometry, particularly at the leading and trailing edges.

The total mass of the coating is 0.65 kg, the same amount as prototype A. The list of materials for prototype B is shown in Table 4.

Table 4. List of materials for prototype B.

Material	Commercial data
UD-FG	SAERTEX U-E-1180 gsm (SAERTEX, 2022)
BX-FG	SAERTEX X-E-830 gsm (SAERTEX, 2022)
Epoxy resin matrix	KUKDO epoxy systems (KUKDO, 2011)
Epoxy structural adhesive	HEXION EPIKOTE™ MGS™ BPR 135G-Series (HEXION/Westlake Epoxy, 2023)
Coating	Polyurethane paint COMEX (COMEX, 2024)

Prototype C – VARTM Manufacturing Process

Prototype C involves the integration of a shear-web element by replacing the EPS core of Prototype B with a polyurethane (PU) core. This modification results in an increase in weight due to the added structural adhesive and epoxy resin. Prototype C follows the same four-layer fiberglass lamination as Prototype B. This PU core functions as a shear-web, providing an additional bonding point and enhancing the stiffness of the blade, as illustrated in Figure 11. The PU core includes an internal fiberglass bridge that further increases the stiffness of the composite structure (SAERTEX, 2022).

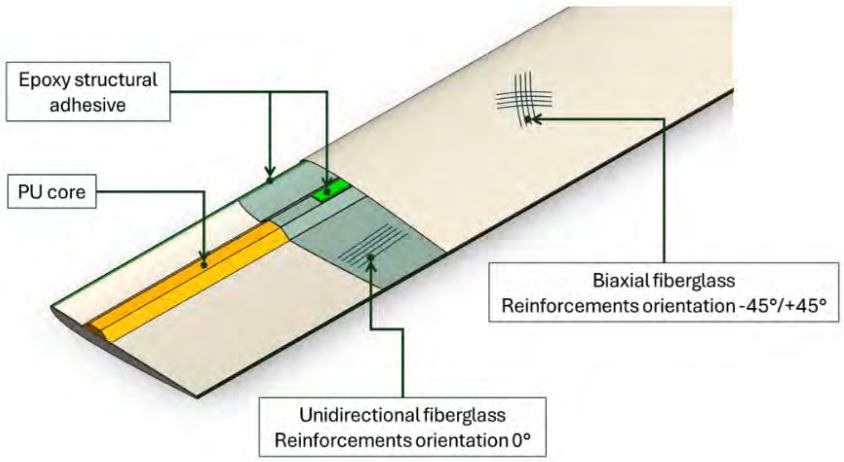

Figure 11. Structural design of prototype C

C-1) The manufacturing process of Prototype C is identical to that of Prototype B. After stacking and aligning the three BX-FG layers on the mold, the PU core is placed prior to adding the UD-FG layer, which is aligned with the pitch axis of the blade and centered on the PU core. The PU core has a geometry of 2 m in length, 75 mm in width, and 10 mm in thickness, as illustrated in Figure 12. The PU core is covered with a UD-FG layer, verifying that it does not move from its position. The PU core has a density of 214 kg/m^3, this material gives an extra mass to the entire shell of 0.32 kg.

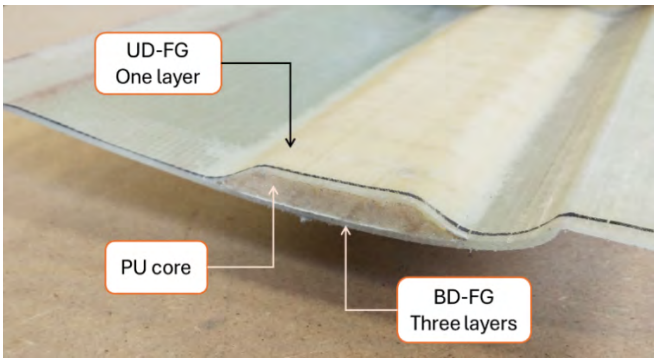

Figure 12. PU core lamination of prototype C.

The total mass of a BX-FG layer is 2.1 kg and for UD-FG it is 1.4 kg. The total mass of the dry fiberglass layers is 3.5 kg for the entire shell.

C-2) Based on a fiber volume fraction (FvF) of 100:50 for the infusion process, the total mass of the epoxy resin matrix for each shell is 1.75 kg. The VARTM process was performed following the same procedure as for Prototype B, using the same consumable arrangement for resin infusion and a curing process of 10 hours at 80 °C for each shell.

C-3) or Prototype C, bond lines of epoxy structural adhesive were applied to the inner surface of Shell 1. The first bond line was applied along the perimeter, and the second bond line was applied along the PU core section, as illustrated in Figure 13. The second bond line provides adhesion with Shell 2 and simulates the shear-web within the blade. The total mass of structural adhesive used is 1.0 kg. The curing process was carried out at 80 °C for 10 hours. Shell 2 is then placed over Shell 1, and uniform pressure is applied across the entire surface to ensure proper bonding. Any excess epoxy structural adhesive that bled around the edges is removed during the trimming process. A complete list of materials used for Prototype C is presented in Table 5.

The total mass of the coating of prototype C is 0.65 kg, the same amount as prototype A.

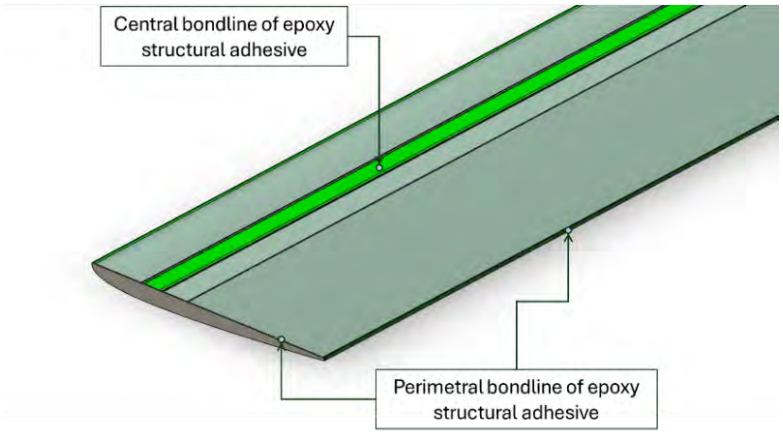

Figure 13. Epoxy structural adhesive bond lines.

Table 5. List of materials for prototype C.

Material	Commercial data
UD-FG	SAERTEX U-E-1180 gsm (SAERTEX, 2022)
BX-FG	SAERTEX X-E-830 gsm (SAERTEX, 2022)
Epoxy resin matrix	KUKDO epoxy systems (KUKDO, 2011)
PU core	SAERfoam ® 80 Series (SAERTEX, 2022)
Epoxy structural adhesive	HEXION EPIKOTE™ MGS™ BPR 135G-Series (HEXION/Westlake Epoxy, 2023)
Coating	Polyurethane paint COMEX (COMEX, 2024)

Results and Discussion

Mass results

Based on the data obtained from each manufactured prototype, the total mass of each prototype is presented in the Table 6.

Comparing the mass of individual materials and the total mass of each prototype, Prototype A is the lightest at 5.11 kg, Prototype B has a total mass of 5.81 kg, and Prototype C is the heaviest at 7.22 kg. The difference in mass between Prototype A, manufactured manually, and Prototype B, produced using the VARTM method, represents an increase of approximately 13%; while the inclusion of the internal reinforcement in Prototype C results in an increase of approximately 41%.

Table 6. Comparison of materials masses for prototypes A, B and C.

Material	Prototype A	Prototype B	Prototype C
UD-FG	-	1.00 kg	1.40 kg
BX-FG	0.71 kg	2.10 kg	2.10 kg
Epoxy resin matrix	1.20 kg	1.56 kg	1.75 kg
EPS core	1.10 kg	-	-
PU core	-	-	0.32 kg
Epoxy filler	1.45 kg	-	-
Epoxy structural adhesive	-	0.5 kg	1.00 kg
Coating	0.65 kg	0.65 kg	0.65 kg
Total	**5.11 kg**	**5.81 kg**	**7.22 kg**

Comparing Prototypes B and C, the increase in mass is attributed to the additional UD-FG layer, the increased epoxy resin required for the PU core, the PU core itself, and the second bond line. Prototype C has approximately 24% greater mass than Prototype B, considering that both prototypes were fabricated using the VARTM process and with a controlled fiber volume fraction (FvF) of 100:50.

Furthermore, the integration of the shear-web component in Prototype C results in a twofold increase in the mass of epoxy structural adhesive.

Cost analysis

The commercial materials used in the manufacture of these prototypes are considered specialized, as they are intended for wind industry applications and are certified by Det Norske Veritas (DNV) and Germanischer Lloyd (GL). Mexico does not have domestic manufacturers capable of supplying these materials; consequently, the associated costs are higher compared to other countries and relative to standard commercial fiberglass and resin matrices.

Based on the list of materials for each manufactured prototype, the corresponding cost percentages are presented in Table 7.

Table 7. Comparison of manufacturing cost percentages for Prototypes A, B, and C. Costs referenced to 2024

Material	Prototype A	Prototype B	Prototype C
UD-FG	0%	12%	17%
BX-FG	9%	27%	27%
Epoxy resin matrix	67%	87%	97%
EPS core	6%	0%	0%
PU core	0%	0%	7%
Epoxy filler	3%	0%	0%
Epoxy structural adhesive	0%	74%	148%
Coating	15%	15%	15%
Total	**100%**	**215%**	**312%**

When comparing the cost of each prototype, Prototype A is used as the cost reference. From this, it can be deduced that Prototype B costs more than twice as much as Prototype A, while Prototype C is nearly three times the cost. The

difference between Prototypes B and C is approximately one-third, which accounts for the inclusion of the PU core and the corresponding increases in structural adhesive and UD fiberglass.

According to Table 7, the epoxy resin used in Prototype A is the most expensive component. For Prototype B, the costs are distributed between the resin and the structural adhesive. In contrast, for Prototype C, the resin accounts for approximately one-third of the total cost, while the structural adhesive represents nearly half of the total cost. This could be one of the reasons why hundreds of thousands of euros are invested in Europe for research and technological development of structural adhesives for use in composite materials in the offshore energy and aerospace industries (Budzik et al., 2021). From the same table, it can be observed that the costs associated with the cores (EPS and PU) and the epoxy filler have a minimal impact on the total cost, while the coating is consistent across all prototypes. A notable difference lies in the number and type of fibers required to ensure structural strength, which is beyond the scope of this document.

Based on the hand lay-up and VARTM processes for blade manufacturing, several key characteristics of each process can be identified, as summarized in Table 8.

Table 8. Comparison of the VAWT blade prototype manufacturing process.

Parameter	**Hand lay-up process**	**VARTM process**
Mass	For the hand lay-up process (Prototype A), the fiber volume fraction (FvF) ratio used was 100:169, meaning that for every 100% of fiber mass, an additional 169% of resin mass was required. Therefore, any prototype manufactured by the manual method will primarily depend on the determination of its reinforcement mass (UD and BX fiberglass).	In the VARTM process, the FvF ratio is maintained at 100:50, and this relationship can be effectively controlled by the vacuum applied during the infusion setup. In other words, 100% of the fiber mass is complemented by only 50% of the resin mass.
Costs and materials	This method does not require specialized laboratories, equipment, or tools. It also allows the use of non-structural fibers (short fiber reinforcements) and different types of resins (e.g., polyester).	Structural fiberglass (continuous fiber reinforcements) and consumables significantly increase the manufacturing cost. In addition, the VARTM process requires a specialized facility equipped with tools and equipment such as vacuum pumps, a trimming room, a curing oven, and a storage room for materials.
Manufacturing time	The manufacturing time is relatively short. For Prototype A, the total manufacturing time was 32 hours, including the surface repair with epoxy filler and the painting process.	For the VARTM process, the manufacturing time of each prototype (B and C) was 48 hours, as this method involves more steps in blade fabrication. Prototype C required an additional 2 hours due to the integration of the PU core.
Surface quality	For Prototype A, surface repair was necessary because the epoxy resin slid due to the effects of gravity before curing, as shown in Figure 14-(a). This repair increased the mass to 1.45 kg, generating an imbalance.	The VARTM process delivers a shell with fewer defects, requiring only minor repairs, as shown in Figure 14-(b). In addition, the vacuum bag ensures uniform impregnation of the epoxy resin matrix into the glass fiber layers.

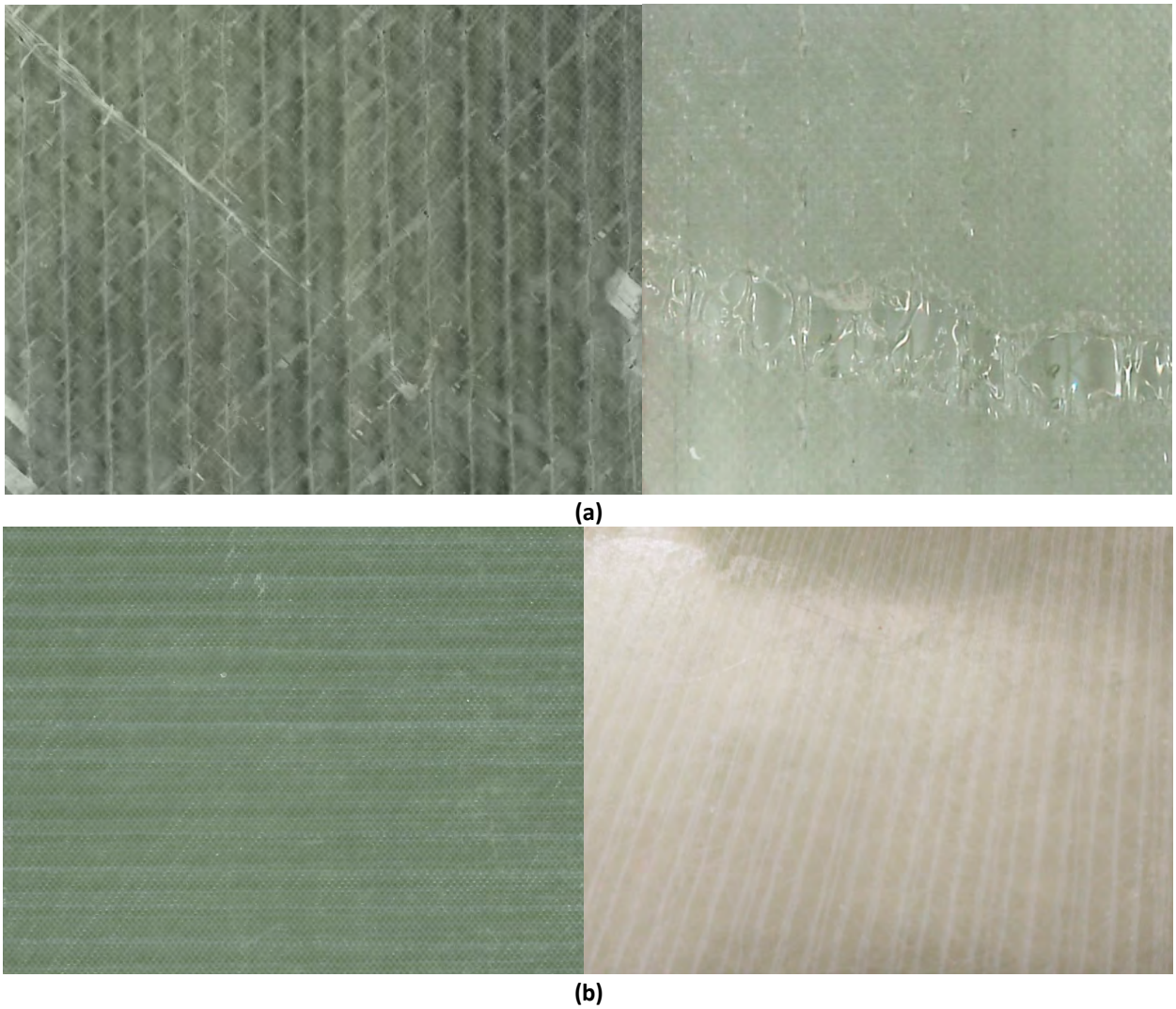

Figure 14. (a) Hand lay-up external surface quality, and (b) VARTM external surface quality.

Conclusions

This research compared the mass, cost, and surface quality of three VAWT blade prototypes, manufactured using both hand lay-up and Vacuum Assisted Resin Transfer Molding (VARTM) processes, with the goal of identifying the material costs and mass of the blades in order to optimize their manufacturing process.

Key findings regarding mass indicated that Prototype A, produced via hand lay-up with an EPS core, was the lightest at 5.11 kg. Prototypes B and C, both manufactured using the VARTM process, were successively heavier. Prototype B, without a shear web, weighed 5.81 kg, an approximate 13% increase over Prototype A. Prototype C, which incorporated a polyurethane (PU) core as a shear web, was the heaviest at 7.22 kg, representing an increase of about 41% compared to Prototype A and 24% compared to Prototype B. The added mass in Prototype C was attributed to the additional unidirectional fiberglass (UD-FG) layer, increased epoxy resin for the PU core, the PU core itself, and a twofold increase in epoxy structural adhesive mass for the second bond line.

In terms of cost, the hand lay-up process (Prototype A) was the most economical, serving as the cost reference (100%). The VARTM process significantly increased manufacturing expenses, with Prototype B costing 215% and Prototype C nearly three times as much (312%) as Prototype A. Specialized commercial materials, not domestically manufactured in Mexico, contributed to these higher costs. For Prototype A, the epoxy resin was the most expensive component. In contrast, for VARTM prototypes, the costs were distributed between the epoxy resin matrix and, notably, the epoxy structural adhesive, which accounted for almost half of Prototype C's total cost due to the shear web integration. Cores

(EPS and PU) and epoxy filler had a minimal impact on the total cost, while coating costs were consistent across all prototypes.

Regarding manufacturing process characteristics and quality, the hand lay-up method (Prototype A) required less specialized equipment and was generally faster (32 hours) but resulted in a rough surface due to gravity-induced resin sliding, necessitating surface repair with epoxy filler and leading to a high resin-to-fiber ratio (FvF of 100:169). Conversely, the VARTM process (Prototypes B and C) yielded shells with superior surface quality and fewer defects, largely due to uniform resin impregnation ensured by the vacuum bag and controlled FvF (100:50). However, VARTM required specialized facilities, more consumables, and a longer manufacturing time (48 hours for B and 50 hours for C), contributing to its higher cost.

This study underscores a critical trade-off between manufacturing cost and blade mass. While hand lay-up offers a cost-effective solution for lighter blades, it compromises on surface quality and precise material control. VARTM, though more expensive and resulting in heavier blades (especially with structural enhancements), delivers superior quality and better material utilization, which are vital for enhancing efficiency and durability. The significant cost contribution of structural adhesives highlights an area for future research and development to potentially reduce overall manufacturing expenses in high-performance composite applications, echoing investment trends observed in Europe. Ultimately, the choice of manufacturing process should align with the specific performance requirements and economic constraints of VAWT applications, particularly those intended for challenging urban environments or offshore installations.

Considering that the criteria for selecting the optimal option are manufacturing quality, low cost, and minimal mass, based on the findings of Vidal-Flores and Hernández-Arriaga (2024), which show that lower blade mass enables rotor start-up at lower wind speeds, Prototype B was selected as the best option for the fabrication of an H-type VAWT rotor, with an average mass of 5.81 kg per blade. It is important to mention that the mechanical characterization of the proposed blades through static and dynamic tests is part of another practical study aimed at confirming theoretical concepts. The VARTM process allows for standardized and more controlled surface quality improvements compared to the hand lay-up method, which relies on manual lamination and must be adapted for each individual piece. Furthermore, the cost of Prototype B could potentially be reduced by approximately 30% through a redesigned manufacturing process, which is currently under investigation and includes a patent proposal for ultralight, one-shot blades to be reported in future work.

Other options to enable the development of VAWT blade designs with different materials, such as natural fibers (sisal, flax, hemp, jute, etc) are under research focusing on reuse after their life cycle. The goal remains to reduce costs and implement advanced technologies in composite manufacturing processes, while also introducing a circular economy for VAWTs. This approach aims to make these turbines more accessible and affordable for use in urban environments.

Acknowledgments and Funding: The authors would like to thank the Laboratorio de Innovación en Energía Eólica de CIATEQ A. C. Bernardo Quintana Querétaro unit for allowing the use of its facilities and equipment for the development of this work and the Secretaría de Ciencia, Humanidades, Tecnología e Inoovación (SECIHTI).

Author contributions: G.V.-F.: writing, conceptualization, provide materials, design, editing, supervision, project administration; F.Q.-E.: writing, analysis and interpretation of data, conceptualization, provide materials, design, data collection, editing. J.R. G-B: manufacture of prototypes, provide materials, analysis and interpretation of data, writing, editing. I.A.-M: manufacture of prototypes, provide materials, analysis and interpretation of data, writing, editing.

References

Alvarado, M. I. (2023). Análisis aeroelástico de detalle para el rediseño estructural del laminado con materiales compuestos de un aspa para un aerogenerador de 30 kW. UAEMéx: Universidad Autónoma del Estado de México.

Bai, T., Liu, J., Zhang, W., & Zou, Z. (2014). Effect of surface roughness on the aerodynamic performance of turbine blade cascade. *Propulsion and Power Research*, *3*(2), 82–89, https://doi.org/10.1016/j.jppr.2014.05.001

Boo, S.Y., Shelley, S.A., Griffith, D.T., & Escalera Mendoza, A.S. (2023). Responses of a Modular Floating Wind TLP of MarsVAWT Supporting a 10 MW Vertical Axis Wind Turbine. *Wind*, 3, 513–544, https://doi.org/10.3390/wind3040029

Brandetti, L. (2024). Design for urban vertical-axis wind turbines: balancing performance and noise. TU Delf: Delft University of Technology, https://doi.org/10.4233/uuid:812de44e-36fb-4e5d-acf7-973f38d965de

Budzik, M. K., Wolfahrt, M., Reis, P., Kozłowski, M., Sena-Cruz, J., Papadakis, L., Nasr Saleh, M., Machalicka, K. V., Teixeira de Freitas, S., & Vassilopoulos, A. P. (2021). Testing mechanical performance of adhesively bonded composite joints in engineering applications: an overview. *Journal of Adhesion*, *98*(14), 2133-2209, https://doi.org/10.1080/00218464.2021.1953479

Chawla, K. K. (2019). Composite materials: science and applications (4th ed). Springer.

COMEX. (2024). Carta técnica: U-10 Recubrimiento de Poliuretano de Altos Sólidos. [Archivo PDF], https://www.comex.com.mx/getattachment/f5bca495-8d9a-42d2-92e8 a83c9ce7292c/.aspx/. Consultado el 24 de febrero de 2024.

Cuevas-Carvajal, N., et al. (2022). Effect of geometrical parameters on the performance of conventional Savonius VAWT: A review. *Renewable and Sustainable Energy Reviews*, 161, 112314, https://doi.org/10.1016/j.rser.2022.112314

Devin, M., Mendoza, N., Platt, A., Moore, K., Jonkman, J., & Ennis, B. (2023). Enabling Floating Offshore VAWT Design by Coupling OWENS and OpenFAST: Article No. 2462. *Energies*, *16*(5), https://doi.org/10.3390/en16052462

Edwards, E. C., Holcombe, A., Brown, S., Ransley, E., Hann, M., & Greaves, D. (2024). Trends in floating offshore wind platforms: A review of early-stage devices. *Renewable and Sustainable Energy Reviews*, *193*, 114271, https://doi.org/10.1016/j.rser.2023.114271

Geneid, A.A., Atia, M.R.A. & Badawy, A. (2022). Multi-objective optimization of vertical-axis wind turbine's blade structure using genetic algorithm. *Journal of Engineering and Applied Science, 69*, 90, https://doi.org/10.1186/s44147-022-00150-z

Ghigo, A., Faraggiana, E., Giorgi, G., Mattiazzo, G., & Bracco, G. (2024). Floating Vertical Axis Wind Turbines for offshore applications among potentialities and challenges: A review. *Renewable and Sustainable Energy Reviews*, 193, 114302, https://doi.org/10.1016/j.rser.2024.114302

Gurit. (2016). Guide to Composites: Delivering the future of composite solutions. Gurit

HEXION/Westlake Epoxy. (2023). Technical data sheet: EPIKOTETM Resin MGS ® 135G-Series

IEC. (2013). IEC 61400-2 Wind turbines – Part 2: Small wind turbines (edition 3.0).

IRENA. (2012). RENEWABLE ENERGY TECHNOLOGIES: COST ANALYSIS SERIES – Volume 1: Power sector Issue 5/5 Wind Power, https://www.irena.org/-/media/Files/IRENA/Agency/Publication/2012/RE_Technologies_Cost_Analysis-WIND_POWER.pdf. Consultado el 24 de octubre de 2024.

Juan, Y., Rezaeiha, A., Montazeri, H., Blocken, B., & Yang, A. (2024). Improvement of wind energy potential through building corner modifications in compact urban areas. *Journal of Wind Engineering and Industrial Aerodynamics*, *248*, 105710, https://doi.org/10.1016/j.jweia.2024.105710

KUKDO. (2011). Technical data sheet: KUKDO Epoxy systems for composites. KUKDO CHEMICAL. CO., LTD.

Lee, C.H., Khalina, A., Nurazzi, et al (2021). The Challenges and Future Perspective of Woven Kenaf Reinforcement in Thermoset Polymer Composites in Malaysia: A Review. *Polymers*, *13*, 1390, https://doi.org/10.3390/polym13091390

Marinić-Kragić, I., Vučina, D., & Milas, Z. (2022). Robust optimization of Savonius-type wind turbine deflector blades considering wind direction sensitivity and production material decrease. *Renewable Energy*, *192*, 150-163, https://doi.org/10.1016/j.renene.2022.04.118

Marzec, Ł., Buliński, Z., Krysiński, T., & Tumidajski, J. (2023). Structural optimisation of H-Rotor wind turbine blade based on one-way Fluid Structure Interaction approach. *Renewable Energy*, *216*, 118957, https://doi.org/10.1016/j.renene.2023.118957

Mendoza, V., Katsidoniotaki, E., & Bernhoff, H. (2020). Numerical Study of a Novel Concept for Manufacturing Savonius Turbines with Twisted Blades *Energies, 13*(8), 1874, https://doi.org/10.3390/en13081874

SAERTEX. (2022). Structural core material. [Archivo PDF], https://www.saertex.com/en/support/downloads. Consultado el 10 de febrero de 2022.

SAERTEX. (2022). Technical data sheet: U-E-1182g/m2-1270mm. [Archivo PDF], https://www.saertex.com/en/products/datasheet-glass. Consultado el 10 de febrero de 2024.

SAERTEX. (2022). Technical data sheet: X-E-832g/m2-1270mm. [Archivo PDF], https://www.saertex.com/en/products/datasheet-glass. Consultado el 10 de febrero de 2024.

Stoevesandt, Bernhard & Schepers, Gerard & Fuglsang, Peter & Yuping, Sun. (2020). Handbook of Wind Energy Aerodynamics. Springer.

Vidal-Flores, G., & Hernandez-Arriaga, I. (2024). Optimización aerodinámica para mejorar el par de arranque de una Turbina de Viento de Eje Vertical Savonius-Darrieus de 1 kW. *Revista Ingeniería Mecánica Tecnología y Desarrollo, 7*(5), 109-119. https://doi.org/10.59920/rimtd.20241m

Optimization of anaerobic digestion under psychrophilic conditions using plant biofilms: evaluation of biogas yield and quality in a rural tubular biodigester

Analith Altamirano-Cubas, Gino Alfredo Vergara Medina, Wildor Gosgot Angeles, Roberth Esteve Iliquin-Fernandez *

Centro de Investigación en Climatología, Energías Renovables, Tecnología Ambiental y Construcción Sostenible (CINCERCOS), Instituto de Investigación para el Desarrollo Sustentable de Ceja de Selva (INDES-CES), Universidad Nacional Toribio Rodríguez de Mendoza de Amazonas (UNTRM), Chachapoyas 01001, Perú

* Corresponding author: roberth.iliquin@untrm.edu.pe; Tel.: (+51) 953 613 287

Received: June 11, 2025 Accepted: July 21, 2025 Published: December 13, 2025
DOI: https://doi.org/10.56845/rebs.v7i2.658

Abstract: This study evaluates the performance of a tubular biodigester operating in psychrophilic conditions, incorporating plant lianas as biofilm support to improve the anaerobic digestion of bovine manure. A 12 m^3 biodigestion system was constructed in Chachapoyas, Peru, and loaded with a manure:water mixture (1:5). Physicochemical parameters, the production and quality of biogas, were monitored, and the study applied the Gompertz model to describe the kinetic behavior. The results show that, despite operating at average temperatures of 16.95 °C, the system reached its hydraulic retention time (HRT) in just 15 days, generating 3 m^3 of biogas with a daily production of 0.2–0.3 m^3. Purification reduced H_2S by 75 % and purified methane reached 68.18 %, its suitability for domestic energy use. The Gompertz model adequately adjusted the data (R^2 = 0.9992), projecting a potential production of 3.89 m^3. The use of plant biofilms improved microbial retention and process stability, suggesting a low-cost solution with high replicability in cold rural areas.

Keywords: lianas, HRT, Gompertz, methanogenesis, biofertilizers

Introduction

Biogas, composed mainly of methane and carbon dioxide, is generated by anaerobic digestion (AD), a microbiological process that decomposes organic matter in the absence of oxygen (Ni, 2024; Gerardi, 2003). This technology contributes to mitigating climate change by capturing methane (CH_4) generated during AD, preventing its release into the atmosphere, where it has a global warming potential 23 times greater than CO_2 (Rivas-Solano *et al*., 2016), with a mitigation potential of up to 200 $MtCO_2eq$ per year (Rodríguez-Jiménez *et al*., 2022). This aligns with energy sustainability objectives by partially replacing fossil fuels and reducing emissions associated with their use.

AD is carried out in biodigesters, airtight containers that create anaerobic conditions (Ni, 2024). Their application in rural areas is efficient due to the availability of biodegradable substrates, their low cost and versatility, allowing the treatment of agricultural, food and livestock waste, the generation of clean energy and the reduction of solid waste (Aridi &Yehya, 2024).

In addition, biodigesters generate by-products such as biol and biosol, used as organic fertilizers, improving agricultural yields and rural income (Barrena *et al*., 2019; Martí-Herrero *et al*., 2014). Although this technology was introduced in Latin America in the 1970s and 1980s, its consolidation has occurred recently, with successful results in rural communities (Garfí *et al*., 2016).

There are three main types of small-scale biodigesters: fixed dome, floating drum, and tubular. Fixed dome digesters, often buried to reduce construction costs, experience variations in pressure and efficiency due to changes in temperature and volume (Kinyua *et al*., 2016). In contrast, tubular biodigesters (Taiwanese model) use inexpensive materials such as polyethylene or heat-sealed PVC, incorporate external gasometers, and are common in rural areas, where they operate with volumes of 6 to 10 m^3 (Kinyua *et al*., 2016; Njoki *et al*., 2013; Barrena *et al*., 2019; Ferrer *et al*., 2011).

The efficiency of anaerobic digestion is strongly dependent on temperature. In cold environments, microbial activity is reduced, leading to the accumulation of volatile fatty acids and lower biogas production (Riau *et al*., 2010; Kashyap *et al*., 2003). This challenge is relevant in high Andean regions, where temperatures fluctuate between -15 and 20 °C and extreme events such as frost and cold occur (Álvarez & Lidén, 2008; Poveda *et al*., 2020), affecting health, livestock,

and crops, especially in areas such as southern Peru and the Bolivian Amazon (Marengo *et al*., 2012; Chávez & Takahashi, 2017).

Anaerobic digestion relies on microbial communities that carry out the stages of hydrolysis, acidogenesis, acetogenesis, and methanogenesis (Abendroth *et al*., 2020). The use of biofilms on plants or synthetic supports improves microbial retention, enhancing the production and stability of biogas in cold climates (Gong *et al*., 2011).

This study evaluates a tubular biodigester operated under psychrophilic conditions, using lianas as biofilm support to optimize AD with 1:5 diluted bovine manure. Biogas production, composition and efficiency were analyzed using the modified Gompertz model, demonstrating the viability of this low-cost technology in cold rural areas.

Materials and Methods

Study Area

The experimental site was located on the central campus of the Universidad Nacional Toribio Rodríguez de Mendoza de Amazonas – UNTRM (Figure 1), in Chachapoyas, Peru (6°14'1.3" S; 77°51'7.6" W). The city has a variable climate, with temperatures ranging between 11°C and 26°C, with maximums of 21°C in November and minimums of 7.5°C in August. The highest rainfall occurs in March, with 136.7 mm/month (SENAMHI, 2025).

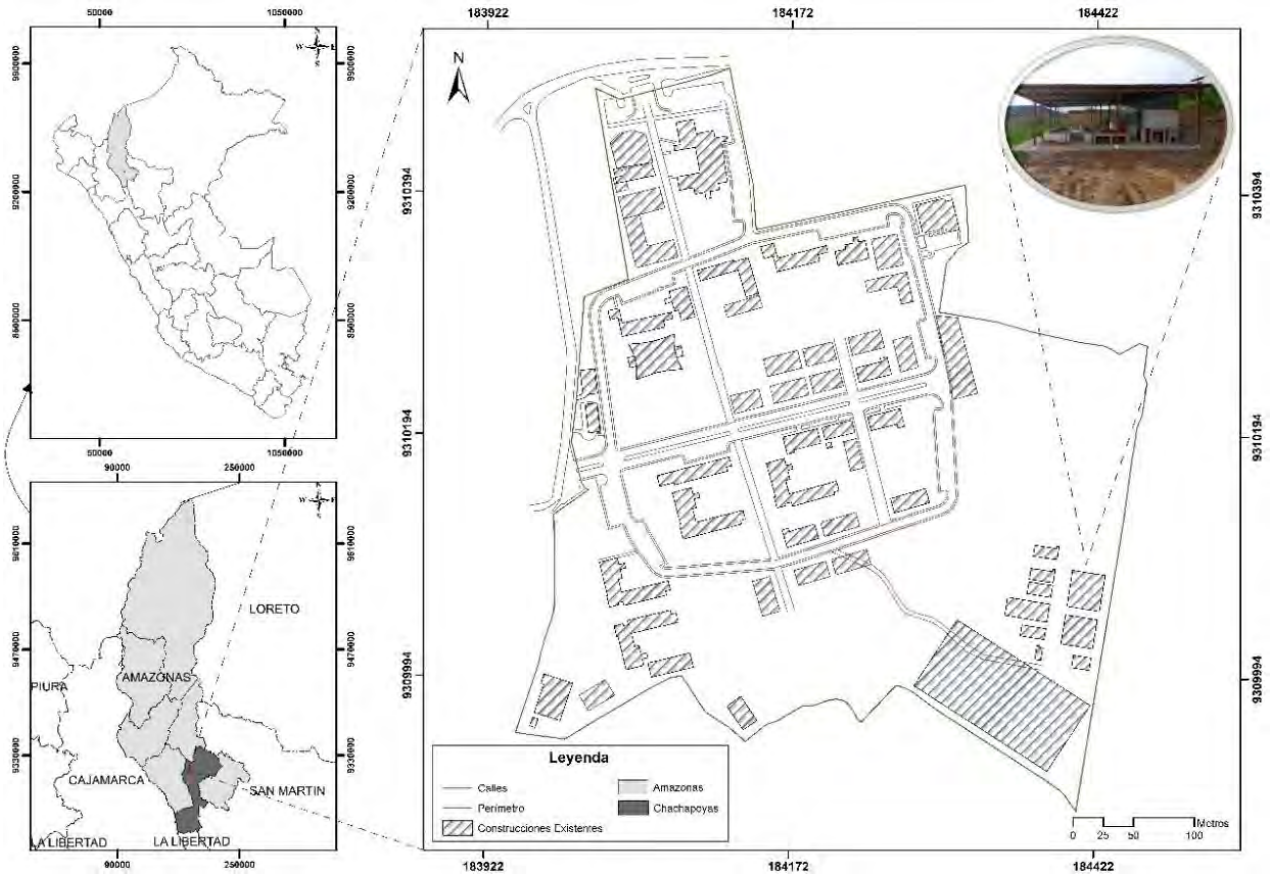

Figure 1. Location of the experimental site

Biogas production system

The biogas production system was designed according to the criteria of Barrena *et al*. (2019) and included a biodigester, a gasometer and a purification and control panel (Figure 2).

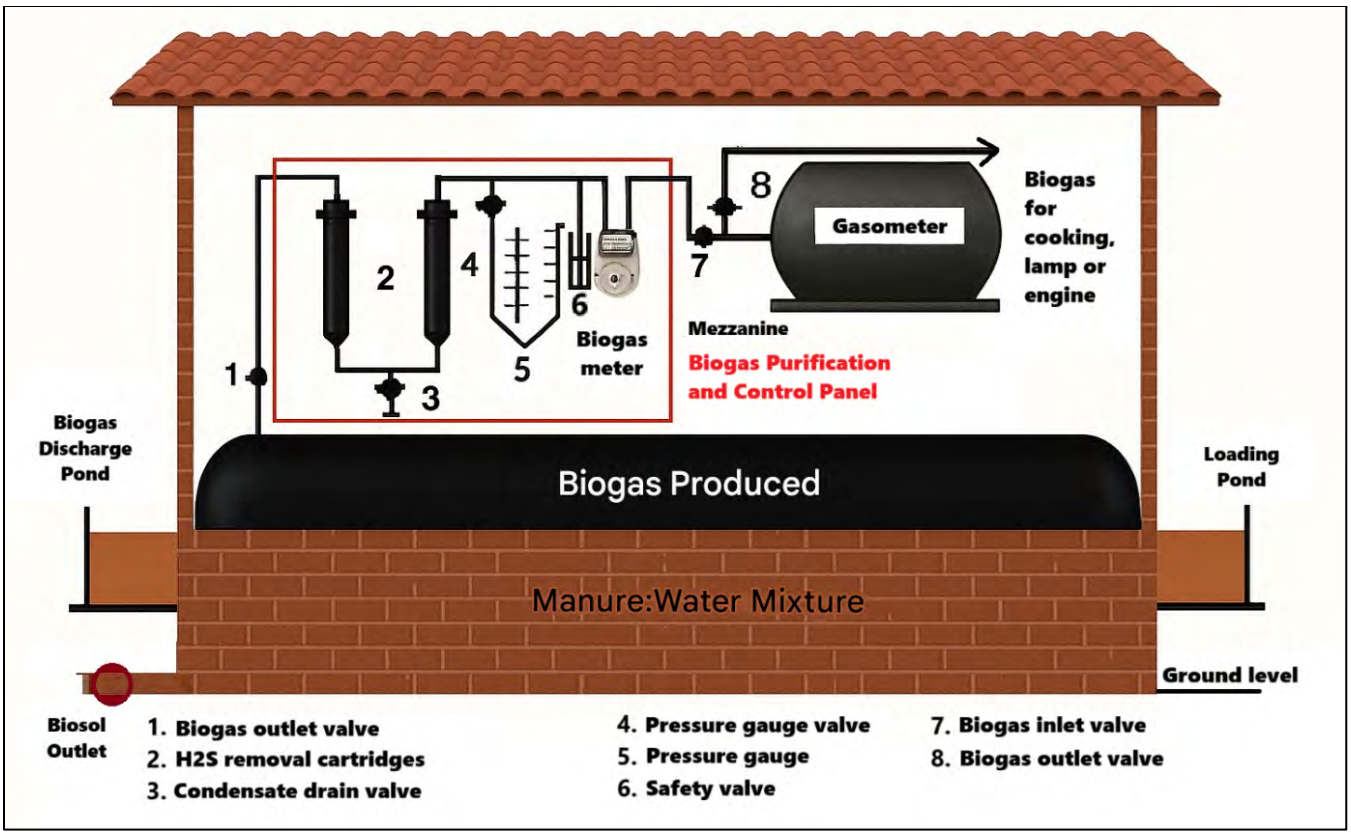

Figure 2. Biodigestion system

The tubular biodigester was built with 1.0 mm thick PVC geomembrane, with a diameter of 1.27 m, a length of 10 m and a total volume of 12 m^3. It had connections for loading, discharging biol and biosol, as well as a top output of biogas by through a nipple and a 1" stopcock.

The gasometer was built with 1 mm thick PVC geomembrane, with dimensions of 1.50 m x 3 m and a volume of 3 m^3. It had a 1" PVC threaded nipple and a 1" stopcock for the inlet and outlet of the biogas. The biogas purification and control panel was consisted of two heavy PVC pipe cartridges 2" and 50 cm long, with reductions to 1/2" at both ends, connected to a bridge with a valve to eliminate condensate water. Each cartridge was filled with 2.5 kg of 2" iron nails and iron sponges at both ends, to remove hydrogen sulfide (H_2S).

The pressure gauge was constructed with a U-shaped 1/4" PVC hose, partially filled with water, whose height difference indicated the biogas pressure. To regulate it, a 3 L plastic bottle with water up to 3/4 of its volume was used, into which the pipe was inserted, marked with grooves every centimeter to facilitate reading.

Installation of lianas as biofilms

Lianas are perennial, herbaceous or woody climbing plants with long and thin stems, their leaves are simple and alternate. These plants are found mainly in Tropical America, widely distributed in tropical and temperate regions (Xu & Chang, 2017).

The lianas were collected in Villa Cocochó (Camporredondo, Luya, Amazonas; 6°11'32" S; 78°19'14" W) and transferred to the experimental site. They were dried for a month to facilitate spherical weaving. Eighty structures were made in the form of bundles or compact baskets of approximately 10 cm in diameter, fixed to a rope with a 5 cm separation between them.

Before installing the biodigester in the pool, the spherically intertwined lianas were introduced using the rope attached to a 1/2" PVC pipe. This assembly was carefully inserted through the loading and unloading holes of the biodigester, ensuring adequate internal distribution of the lianas within the system.

Operating Parameters

For the loading of the biodigester, cattle manure from the UNTRM stable was used as substrate, mixed with water in a 1:5 ratio. To load 9 m³, 45 cylinders of 200 L were prepared, each containing 33.3 kg of manure. Although the mixture was calculated based on weight, the ratio corresponds to 1:5 by volume, considering that the density of manure is close to 1 kg/L (Aremanda *et al*., 2023), meaning that for each part of manure five parts of water were added. The loading was carried out daily with 4 cylinders, and was completed in 12 days. Subsequently, anaerobic digestion was allowed to produce biogas and biofertilizers (biol and biosol).

To measure ambient and biodigester temperature, four Data Loggers Yowexa SSN22ET were installed: at the inlet, center (10 cm deep) and outlet of the biodigester, and outside, on the structure of the gasometer. They recorded temperature every 15 minutes, from 6:00 a.m. to 6:00 p.m., throughout the process until the hydraulic retention time (HRT) was reached. Then, the temperatures of the three points in the biodigester and the environment were averaged. After completing the loading of the biodigester, a sample of the manure-water mixture was collected and its pH was measured with a portable multiparameter meter (model 3620 IDS, WTW brand), which measures the acidity/alkalinity of the substrate on a scale of 0 to 14.

To measure the volume of biogas produced, a diaphragm-type meter G1.6 was installed on the purification board, connected to the 1/2" PVC pipe by two universal joints of the same diameter. This high-precision, low-pressure drop equipment is widely used for reliable measurement of low natural gas flow rates. When the biodigester dome reached its gas capacity, the biogas composition was evaluated using the Multitec 545 equipment to measure CH_4, CO_2, O_2, H_2S and CO. The measurements were made at two points: upstream of the purification panel and at the connection between the gasometer and the pipe to the kitchen.

The hydraulic retention time was defined as the period, in days, from the loading of the biodigester with the manure-water mixture to the observation of biogas accumulation in the biodigester and gasometer. This value was compared with the one estimated by the formula proposed by Barrena *et al*. (2019), based on the ambient temperature conditions, as presented in equation 1:

$$HRT = -44.705\ ln(T) + 160.394 \quad \textbf{(1)}$$

Where T represents the ambient temperature of the location where the biodigester is installed.

Mathematical modelling of cumulative biogas production

The modified Gompertz model, commonly used to model biogas production because it describes the sigmoidal dynamics of biological processes, was applied (Ofon *et al*., 2025) . This model allows researchers to identify the lag phase, exponential growth and stabilization, using equation 2:

$$B(\mathrm{t}) = B_{max} * \exp\left(-exp\left(\frac{R_m * e}{B_{max}}(\lambda - t) + 1\right)\right) \quad \textbf{(2)}$$

Where B(t) is cumulative biogas production at time t, B_{max} is theoretical cumulative biogas production, R_m is maximum biogas production rate, λ lag time or lag phase, and e Euler number.

The Gompertz model was projected up to 40 days, the standard reference value in psychophilic processes with bovine manure. In mesophilic conditions, HRT typically varies between 20 and 40 days, especially when using dry or diluted manure (Song *et al*., 2023).

Energy yield of biogas

The evaluation of energy yield was carried out upon reaching the maximum HRT, using the biogas stored in the gasometer. A two-burner stove adapted for biogas was used, connected by a steel reduction from 1/2" to 3/8" and

secured with a clamp. Potatoes, eggs and water (common foods in rural families) were cooked, and the system recorded the time and volume of biogas consumed.

Results and Discussion

Operating and productive parameters of the biodigester

The operating conditions of the biodigester with liana-based biofilm support were evaluated. Table 1 summarizes the main physical, chemical and productive parameters recorded during the anaerobic digestion process.

Table 1. Parameters obtained in the production of biogas.

Category	Parameter	Value	Unit	Remarks
Operating conditions	Manure-water ratio	1:5	-	Initial mix ratio
	Ambient temperature	19.91	°C	External conditions
	Biodigester temperature	16.95	°C	Thermal efficiency
	pH	7.49	-	Optimal range for methanogenesis
Retention Time	Design	34	Days	Based on theoretical design
	Real	15	Days	Observed in operation
Biogas production	Initial Volume (First 15 Days)	3	m^3	Accumulated
	Daily production	0.2	m^3/day	Average after stabilization
	Initial pressure	12	cm	Water column
	Daily pressure	2.4	cm	Water column

The 1:5 ratio (manure:water) is commonly used because it improves substrate fluidity, facilitates microbial activity, and reduces clogging. In addition, it optimizes biogas production by increasing the accumulated volume and improving its combustion quality (Tian *et al*., 2023). Proper dilution also improves the physical conditions of the system and its energy performance (Hadiyanto *et al*., 2023).

The average ambient temperature was 19.91 °C, as the experiment was carried out in September and October, during the dry season in Chachapoyas, which generates warmer days (Rascón *et al*., 2021). However, this value indicates a low mesophilic range, close to the optimal lower limit for anaerobic digestion (20–45 °C) (Feghhipour *et al*., 2024).

The internal temperature of the biodigester was 16.95 °C, indicating low psychrophilic conditions. Although mesophilic conditions are more favorable owing to the higher microbial diversity than thermophilic digesters (Liu *et al*., 2022), low temperatures reduce microbial activity and affect optimal biogas production (Hadiyanto *et al*., 2023; Liu *et al*., 2022).

Despite the suboptimal temperatures, the use of biofilm as structural support favored biogas production by providing a stable environment for microbial growth (Wu *et al*., 2023). Biofilms improve gas absorption, facilitate metabolic interactions (Zhang *et al*., 2025), and allow biomass to be retained in the reactor for longer, sustaining its performance (Cayetano *et al*., 2022).

The pH recorded (7.49) is within the optimal range for methanogenesis (6.8–8.2) (Lohani & Havukainen, 2018), indicating a good buffer effect of the substrate. This value favors the development of methanogenic archaea, sensitive to pH variations. Outside this range, methane production can be reduced or stopped (Li *et al*., 2025). The chemical equilibrium achieved allowed stable production of biogas in the system.

Although the theoretical design envisaged an HRT of 34 days, according to the formula of Barrena *et al*. (2019), in practice the biodigester dome (3 m^3 remaining) was filled in 15 days, demonstrating a significant improvement. This result is attributed to biofilm, which optimized microbial colonization and accelerated substrate degradation (Mohmed Moffit *et al*., 2025). The use of local lianas as a support represents a low-cost innovation with replicability potential.

Within 15 days of loading the biodigester with manure-water mixture, the dome reached its full capacity, indicating a production of 3 m^3 of biogas. The daily biogas generation started at 0.2 m^3/day, later stabilizing at 0.3 m^3/day, values consistent with domestic biodigesters in cold areas. For comparison, 5 m^3 rural biodigesters tipically produce around 0.2 m^3/m^3·day, which is sufficient to cook 3 to 4 hours a day (Ferrer *et al*., 2015). Production rates of up to 0.5 m^3/day are possible with good design and thermal management, even in cold climates (Ortega-Castro *et al*., 2025).

The biogas pressure reached 12 cm H_2O and stabilized approximately 2.5 cm H_2O during daily operation, enough for a continuous flow to the kitchen without compressors. Pressures between 15–22 cm H_2O are suitable for kitchens in fixed dome systems (Ramaiyulis *et al*., 2021). Stabilization at this lower pressure indicates a balance between production and consumption, avoiding fluctuations that interrupt the flow (Abdurrakhman *et al*., 2024).

The prior homogenization of the mixture was key to ensuring an even distribution of temperature, nutrients and microorganisms, favoring efficient anaerobic digestion (Karne & Bhatkhande, 2022; Lindmark *et al*., 2014). In addition, it avoided inactive areas and improved microbial contact with the substrate, optimizing biogas production (Babaei & Shayegan, 2019).

The use of lianas as biofilms favored a homogeneous distribution of microbial activity, improving cell retention and stabilizing anaerobic digestion (Abera *et al*., 2024). This helped maintain a uniform temperature in the biodigester (Karne & Bhatkhande, 2022) and achieve the effective HRT in 15 days (Figure 3).

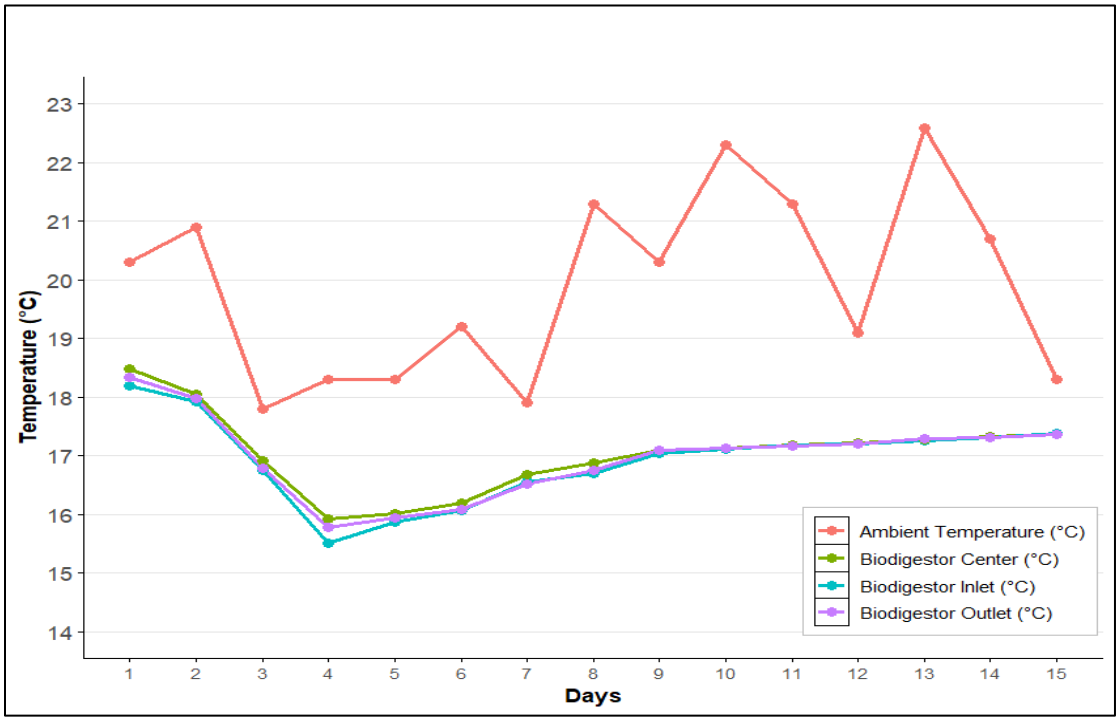

Figure 3. Temperature variation in biodigestion for 15 days

Although the ambient temperature ranged from 18 °C to 23 °C (Figure 3), the internal temperature of the biodigester remained stable between 16 and 17.5 °C until HRT was reached. This indicates that the use of biofilms and adequate homogenization of the substrate enabled an efficient and stable digestion under psychrophilic conditions (Tiwari *et al*., 2021).

Cumulative Biogas Production Curve according to the Gompertz Model

The cumulative production was evaluated until day 15, when the biogas bell was filled. However, in psychrophilic conditions, complete digestion usually requires between 20 and 40 days (Song *et al*., 2023), so the data suggest that

that the process has not reached completion. The measurement was stopped for operational reasons, not because of deplation of production potential

The Gompertz model was adjusted by nonlinear least squares using R software, assigning as initial values the maximum observed production multiplied by two to estimate Bmax, while Rm and λ were set at 0.1 m^3/day and 1 day respectively. These values follow methodological criteria reported in the anaerobic digestion modeling, to facilitate the convergence of the fit and appropriately represent the cumulative biogas production (Kavan Kumar *et al*., 2023).

Figure 4 shows the evolution of the cumulative biogas production, modeled with the Gompertz curve, which characterizes the sigmoidal behavior of anaerobic digestion and allows evaluating its performance over time.

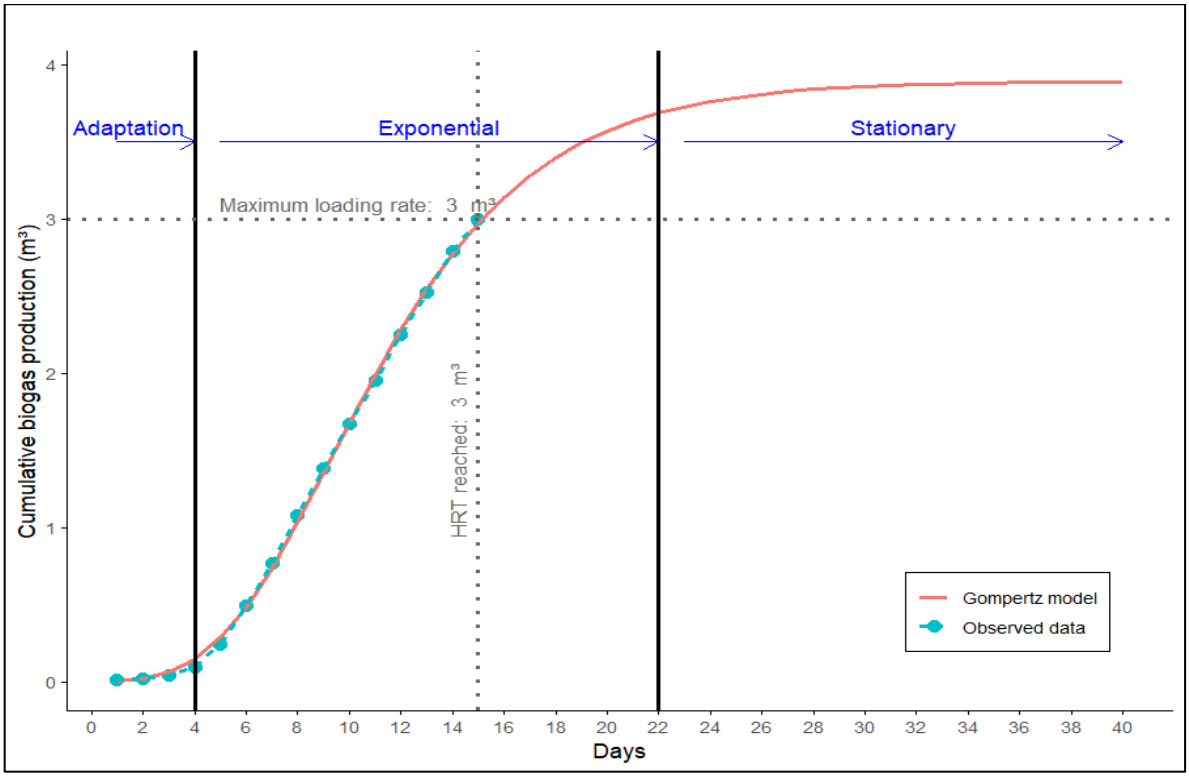

Figure 4. Cumulative growth in biogas production and adjustment with the Gompertz model

At the HRT, the Gompertz curve still displayed a positive slope, indicating that biogas production had not ended. This is common in psychrophilic conditions, where digestion can exceed 30 days (Pilarski *et al*., 2020). Therefore, in experiments where the operation period is truncated, it is necessary to apply models like this one (Esparza-Soto *et al*., 2025).

The production curve showed an adaptation phase (days 1–4) and an exponential phase (days 5–22). Gompertz's model fit well to the data, projecting a total potential of 3.89 m^3 of biogas. Although stabilization was not observed in the field, the model suggests that stabilization would occur beyond the observation window.

Table 2 presents the parameters obtained from the fit of the experimental data to the Gompertz model, which describes the cumulative production of biogas. These values allow characterizing the kinetic behavior of the process and evaluating its efficiency.

The peak generation rate (Rm) of 0.3256 m^3/day indicates an active metabolic phase during digestion. Kinetic models such as the modified Gompertz model reliably estimate this rate with high precision ($R^2 > 0.99$) on various substrates (Adamu *et al*., 2025; Ravikumar *et al*., 2020), confirming the reliability of the value and the consistency of the anaerobic process.

Table 2. Gompertz Model Parameters for Cumulative Biogas Production

Parameter	Estimated value
Bmax	3,893 m^3
Rm	0.3256 m^3/day
λ	4.8441 days
R2	0.9992
T_{80}	15.80 days
T_{90}	19.10 days

The parameter λ represents the initial period of microbial adaptation before the significant start of biogas production. In batch systems at mesophilic temperature, this time typically ranges from 2 to 6 days (Pasalari *et al*., 2021), with high levels of fit to the Gompertz model ($R^2 > 0.99$).

The times T_{80} (15.8 days) and T_{90} (19.1 days), close to the observed HRT, coincide with typical values of mesophilic digestion of organic wastes. In bovine and pig manure, 80-90% of production occurs between 12 and 28 days (Kafle & Chen, 2016), information useful to optimize HRT in continuous and batch systems.

Biogas composition before and after the purification process

Table 3 presents the composition of the biogas before and after its purification, following passage through the cartridges designed to remove hydrogen sulfide (H_2S).

Table 3. Composition and percentage of gases before and after purification.

Gases	Percentage before Purification	Percentage after Purification
CH_4 (%)	71.61	68.18
CO_2 (%)	27.50	17.90
O_2 (%)	0.18	7.99
H_2S (PPM)	624.50	157.40
CO (PPM)	3.50	496.40

Methane (CH_4), the main energy component, showed a slight decrease after purification, going from 71.61% to 68.18%. This reduction is likely attributable to losses during the passage through the cleaning system, which is common in processes where physical or absorbent filters are used (Swinbourn *et al*., 2024). Carbon dioxide (CO_2) decreased significantly from 27.50 % to 17.90 %, demonstrating the effectiveness of the purification system in improving biogas quality. This reduction implies an increase in the calorific value of the final gas, since CO_2 is not combustible (Bahrun *et al*., 2022).

Oxygen (O_2) increased from 0.18% to 7.99%, which may indicate air ingress during the purification process, possibly due to leaks or insufficient system sealing. This increase represents an operational risk, as it can promote the formation of explosive mixtures if the 12% threshold is exceeded (Biogasclean, 2016).

The hydrogen sulfide (H_2S) content was reduced by 75%, from 624.50 to 157.40 ppm, which is beneficial for preventing corrosion in equipment and emissions of toxic compounds (Arıman & Koyuncu, 2022).

Carbon monoxide (CO) increased from 3.50 to 496.40 ppm, indicating possible contamination or unwanted reaction during purification. Although CO is toxic and can affect the calorific value of biogas (Hagos *et al*., 2025; Pera *et al*., 2024), its level remains within the acceptable limit of 1000 ppm (Barrena *et al*., 2019).

Biogas Energy Efficiency Testing

Table 4 shows the three products cooked for four consecutive days. For each one, the cooking time was recorded to calculate the average number of hours required.

Table 4. Cooking time of biogas products

Food	Average Amount	Average Cooking Time (min)
Potato	0.25 kg	24.7 ± 1.2^{a}
Egg	1 unit	12.3 ± 0.9^{b}
Water	1 L	18.5 ± 1.1^{ab}

The values are expressed as mean ± standard deviation (n = 4). Different letters indicate significant differences according to Tukey's test ($p \leq 0.05$).

The energy efficiency of biogas for cooking common foods was evaluated. Potatoes required the most time (24.7 ± 1.2 min), followed by water (18.5 ± 1.1 min) and eggs (12.3 ± 0.9 min). The ANOVA and Tukey's test showed significant differences between potatoes and eggs ($p \leq 0.05$), but not between water and the other two.

The longer cooking time of the potato is due to its greater density and thermal requirement (Marle, 1997), while the egg, due to its lower mass and soft structure, cooks faster (Phisics, 2025).

Boiling 1 liter of water is a good indicator of the thermal performance of biogas, as it is directly related to its methane content (Nallamothu *et al*., 2013). The system allowed 1 liter of water to boil in less than 20 minutes, meeting the standard for domestic efficiency (Petro, 2020).

The average cooking times indicate that the biogas generated has an adequate calorific value for basic uses, comparable to LPG in rural contexts (Shinde *et al*., 2024).

Typical biogas consumption in a domestic burner is 0.34–0.45 m^3/h, with efficiencies of 59–68% (Rajendran *et al*., 2012). In countries such as China, India and Kenya, minimum consumption of 0.38, 0.45 and 0.50 m^3/h, respectively, is reported (Kasinath *et al*., 2021). Thus, the 3 m^3 generated could supply about 3.6 days of domestic use, allowing cooking for 3 to 4 hours a day for a family of 4 to 5 people.

Being a batch system, the biodigester requires daily refills after reaching HRT to maintain continuous biogas production and mass flow (Barrena *et al*., 2019). Therefore, a mixture of 200 liters should be added daily in a manure:water ratio of 1:5, equivalent to about 33.3 kg of fresh manure.

Conclusions

The use of lianas as biofilm support significantly improved microbial retention and allowed stable anaerobic digestion under psychrophilic conditions. This shortened the hydraulic retention time to 15 days, demonstrating an efficient and low-cost solution for cold rural areas.

The manure:water mixture in a 1:5 ratio ensured good substrate fluidity and optimal pH (7.49), which favored methanogenic activity. This chemical condition was essential to stable biogas production in a low-temperature environment.

The biogas produced showed high energy quality, with more than 68% methane after purification and a significant reduction in H_2S. Its use in domestic cooking showed efficiency comparable to LPG, validating its rural applicability.

Gompertz's model accurately described the cumulative biogas production ($R^2 = 0.9992$), identifying key phases of the process. Its application enables the projection of performance and optimization of operating times in similar systems.

The Gompertz curve showed that biogas production continued after day 15, indicating that the process did not fully stabilize. This interruption was due to the limited capacity of the gasometer and not to the depletion of the substrate. Removing the material at this point may result in partially digested material, with risks for its use as biofertilizer. Therefore, it is suggested to expand the storage volume and extend the operation time to fully harness the production potential and ensure stable effluent.

As it is a batch system, daily refilling is essential after TRH is reached to maintain continuous biogas production. Therefore, rural families should be aware of the need to feed the biodigester regularly with the right mixture, thus ensuring a constant and efficient supply of energy.

Acknowledgments and Funding: We would like to the Centro de Investigación en Climatología, Energías Renovables, Tecnología Ambiental y Construcciones Sostenibles (CINCERCOS) and Instituto de Investigación para el Desarrollo Sustentable de Ceja de Selva (INDES-CES) of the Universidad Nacional Toribio Rodríguez de Mendoza de Amazonas of Perú.

Author contributions: A.A.-C.: writing, data collection, analysis and interpretation of data; G.A.V.M.: editing, conceptualization and data analyses; W.G.A.: editing, supervision, project administration and analysis of data, R.E.I-F: writing, conceptualization, interpretation and data analysis.

References

Abdurrakhman, A., Sutiarso, L., Ainuri, M., Ushada, M., & Islam, M. P. (2024). Design of a pressure control system in biogas reactor based on PID controller with Ziegler–Nichols and auto tuning PSO. *Jurnal Otomasi Kontrol dan Instrumentasi, 16*(2), 104–116. https://doi.org/10.5614/JOKI.2024.16.2.5

Abendroth, C., Latorre-Pérez, A., Porcar, M., Simeonov, C., Luschnig, O., Vilanova, C., & Pascual, J. (2020). Shedding light on biogas: Phototrophic biofilms in anaerobic digesters hold potential for improved biogas production. *Systematic and Applied Microbiology, 43*(1), 126024. https://doi.org/10.1016/j.syapm.2019.126024

Abera, G. B., Trømborg, E., Solli, L., Walter, J. M., Wahid, R., Govasmark, E., Horn, S. J., Aryal, N., & Feng, L. (2024). Biofilm application for anaerobic digestion: A systematic review and an industrial scale case. *Biotechnology for Biofuels and Bioproducts, 17*(1), 1–20. https://doi.org/10.1186/s13068-024-02592-4

Adamu, A. A., James, J. G., Olupinla, F. S., & Iyanda, P. O. (2025). Modelling biogas production from organic waste substrates using the Gompertz equation: Parameter estimation and methane composition analysis (Issue 1).

Alvarez, R., & Lidén, G. (2008). The effect of temperature variation on biomethanation at high altitude. *Bioresource Technology, 99*(15), 7278–7284. https://doi.org/10.1016/j.biortech.2007.12.055

Aremanda, R. B., Debretsion, S., Tesfalem, S., & Menghisteab, R. (2023). Competence of cow manure as a sustainable feedstock for bioenergy and biofertilizer production. *International Journal on Food, Agriculture and Natural Resources, 4*(2), 59–67. https://doi.org/10.46676/ij-fanres.v4i2.135

Aridi, R., & Yehya, A. (2024). Anaerobic biodigesters heating sources: Analysis and recommendations. *Renewable and Sustainable Energy Reviews, 202*, 114700. https://doi.org/10.1016/j.rser.2024.114700

Arıman, S., & Koyuncu, S. (2022). Removal of hydrogen sulfide in biogas from wastewater treatment sludge by real-scale biotrickling filtration desulfurization process. *Water Practice and Technology, 17*(7), 1406–1420. https://doi.org/10.2166/wpt.2022.072

Babaei, A., & Shayegan, J. (2019). Effects of temperature and mixing modes on the performance of municipal solid waste anaerobic slurry digester. *Journal of Environmental Health Science and Engineering, 17*(2), 1077–1084. https://doi.org/10.1007/s40201-019-00422-6

Bahrun, M. H. V., Bono, A., Othman, N., & Zaini, M. A. A. (2022). Carbon dioxide removal from biogas through pressure swing adsorption – A review. *Chemical Engineering Research and Design, 183*, 285–306. https://doi.org/10.1016/j.cherd.2022.05.012

Barrena, M. A., Maicelo, J. L., Gamarra, O. A., Oliva, M., Leiva, S., Taramona, L. A., Huanes, M. A., & Ordinola, C. M. (2019). Biogas production and applications.

Biogasclean. (2016). *Safe injection of air or pure oxygen into biogas*. Recuperado de https://www.biogasclean.com

Cayetano, R. D. A., Kim, G. B., Park, J., Yang, Y. H., Jeon, B. H., Jang, M., & Kim, S. H. (2022). Biofilm formation as a method of improved treatment during anaerobic digestion of organic matter for biogas recovery. *Bioresource Technology, 344*, 126309. https://doi.org/10.1016/j.biortech.2021.126309

Chavez, S. P., & Takahashi, K. (2017). Orographic rainfall hot spots in the Andes–Amazon transition according to the TRMM precipitation radar and in situ data. *Journal of Geophysical Research, 122*(11), 5870–5882. https://doi.org/10.1002/2016JD026282

Esparza-Soto, M., Alcaraz-Ibarra, S., Lucero-Chávez, M., Jiménez-Moleón, M. del C., Mier-Quiroga, M. de los A., & Fall, C. (2025). First derivative of Gompertz equation: Identification of substrate fractions in psychrophilic anaerobic digestion. *Biocatalysis and Agricultural Biotechnology, 66*, 103595. https://doi.org/10.1016/j.bcab.2025.103595

Feghhipour, S. E., Hatamipour, M. S., Amiri, H., & Nosrati, M. (2024). Continuous biogas production and ex-situ biomethanation in a trickling bed bioreactor under mesophilic and thermophilic conditions. *Process Safety and Environmental Protection, 190*, 1440–1449. https://doi.org/10.1016/j.psep.2024.07.095

Ferrer, I., Gamiz, M., Almeida, M., & Ruiz, A. (2009). Pilot project of biogas production from pig manure and urine mixture at ambient temperature in Ventanilla (Lima, Peru). *Waste Management, 29*(1), 168–173. https://doi.org/10.1016/j.wasman.2008.02.014

Ferrer, I., Garfí, M., Uggetti, E., Ferrer-Martí, L., Calderón, A., & Velo, E. (2011). Biogas production in low-cost household digesters at the Peruvian Andes. *Biomass and Bioenergy, 35*(5), 1668–1674. https://doi.org/10.1016/j.biombioe.2010.12.036

Ferrer, I., Uggetti, E., Poggio, D., Martí, J., & Velo, E. (2015). *Production of biogas from organic waste in low-cost biodigesters*. Recuperado de http://www.upc.edu/grecdh

Garfí, M., Martí-Herrero, J., Garwood, A., & Ferrer, I. (2016). Household anaerobic digesters for biogas production in Latin America: A review. *Renewable and Sustainable Energy Reviews, 60*, 599–614. https://doi.org/10.1016/j.rser.2016.01.071

Gerardi, M. H. (2003). *The microbiology of anaerobic digesters*. https://doi.org/10.1002/0471468967

Gong, W. J., Liang, H., Li, W. Z., & Wang, Z. Z. (2011). Selection and evaluation of biofilm carrier in anaerobic digestion treatment of cattle manure. *Energy, 36*(5), 3572–3578. https://doi.org/10.1016/j.energy.2011.03.068

Hadiyanto, H., Octafalahanda, F. M., Nabila, J., Jati, A. K., Christwardana, M., Kusmiyati, K., & Khoironi, A. (2023). Preliminary observation of biogas production from a mixture of cattle manure and bagasse residue in different composition variations. *International Journal of Renewable Energy Development, 12*(2), 390–395. https://doi.org/10.14710/ijred.2023.52446

Hagos, G. K., Golie, W. M., Belete, F. A., & Gidey, Y. H. (2025). Biogas upgrading produced through anaerobic co-digestion of organic biowastes: A comparative study. *Biomass Conversion and Biorefinery*, 1–23. https://doi.org/10.1007/s13399-025-06757-5

Kafle, G. K., & Chen, L. (2016). Comparison on batch anaerobic digestion of five different livestock manures and prediction of biochemical methane potential (BMP) using different statistical models. *Waste Management, 48*, 492–502. https://doi.org/10.1016/j.wasman.2015.10.021

Karne, H., & Bhatkhande, D. (2022). Effect of mixing and agitator type on biogas production from food waste in a pilot plant digester. *Waste and Biomass Valorization, 13*(4), 1885–1895. https://doi.org/10.1007/s12649-021-01633-5

Kashyap, D. R., Dadhich, K. S., & Sharma, S. K. (2003). Biomethanation under psychrophilic conditions: A review. *Bioresource Technology, 87*(2), 147–153. https://doi.org/10.1016/S0960-8524(02)00205-5

Kasinath, A., Fudala-Ksiazek, S., Szopinska, M., Bylinski, H., Artichowicz, W., Remiszewska-Skwarek, A., & Luczkiewicz, A. (2021). Biomass in biogas production: Pretreatment and codigestion. *Renewable and Sustainable Energy Reviews, 150*, 111509. https://doi.org/10.1016/j.rser.2021.111509

Kavan Kumar, V., Mahendiran, R., Subramanian, P., Karthikeyan, S., Surendrakumar, A., Kumargouda, V., Ravi, Y., Choudhary, S., Singh, R., & Verma, A. K. (2023). Optimization of biogas potential using kinetic models, response surface methodology, and instrumental evidence for biodegradation of tannery fleshings during anaerobic digestion. *Open Life Sciences, 18*(1). https://doi.org/10.1515/biol-2022-0721

Kinyua, M. N., Rowse, L. E., & Ergas, S. J. (2016). Review of small-scale tubular anaerobic digesters treating livestock waste in the developing world. *Renewable and Sustainable Energy Reviews, 58*, 896–910. https://doi.org/10.1016/j.rser.2015.12.324

Li, S, Ou, X., Wang, D., & Wang, W. (2025). Optimizing biogas production from swine manure: Biogas recirculation coupled with pH adjustment to mitigate lime inhibition. *Process Safety and Environmental Protection, 198*, 107234. https://doi.org/10.1016/j.psep.2025.107234

Lindmark, J., Thorin, E., Bel Fdhila, R., & Dahlquist, E. (2014). Effects of mixing on the result of anaerobic digestion: Review. *Renewable and Sustainable Energy Reviews, 40*, 1030–1047. https://doi.org/10.1016/j.rser.2014.07.182

Liu, Y., Wang, T., Xing, Z., Ma, Y, Nan, F., Pan, L., & Chen, J. (2022). Anaerobic co-digestion of Chinese cabbage waste and cow manure at mesophilic and thermophilic temperatures: Digestion performance, microbial community, and biogas slurry fertility. *Bioresource Technology, 363*, 127976. https://doi.org/10.1016/j.biortech.2022.127976

Lohani, S. P., & Havukainen, J. (2018). Anaerobic digestion: Factors affecting anaerobic digestion process. En *Energy, environment, and sustainability* (pp. 343–359). https://doi.org/10.1007/978-981-10-7413-4_18

Marengo, J. A., Tomasella, J., Soares, W. R., Alves, L. M., & Nobre, C. A. (2012). Extreme climatic events in the Amazon basin. *Theoretical and Applied Climatology, 107*(1–2), 73–85. https://doi.org/10.1007/s00704-011-0465-1

Marle, N. van. (1997). *Characterization of changes in potato tissue during cooking in relation to texture development*.

Martí-Herrero, J., Chipana, M., Cuevas, C., Paco, G., Serrano, V., Zymla, B., Heising, K., Sologuren, J., & Gamarra, A. (2014). Low cost tubular digesters as appropriate technology for widespread application: Results and lessons learned from Bolivia. *Renewable Energy, 71*, 156–165. https://doi.org/10.1016/j.renene.2014.05.036

Mohmed Moffit, M. A., Suja', F., Kabir Ahmad, I., & Bhaskaran, A. N. (2025). Biogas production and reactor performance of a pilot scale anaerobic biofilm digester treating food waste. *Renewable Energy, 243*, 122414. https://doi.org/10.1016/j.renene.2025.122414

Nallamothu, R. B., Teferra, A., & Rao, B. V. A. (2013). *Biogas purification, compression and bottling* (Vol. 2, Issue 6).

Ni, J. Q. (2024). A review of household and industrial anaerobic digestion in Asia: Biogas development and safety incidents. *Renewable and Sustainable Energy Reviews, 197*, 114371. https://doi.org/10.1016/j.rser.2024.114371

Njoki, M. K., Ergas, S. J., Cunningham, J., & Wilkie, A. C. (2013). Effect of solids retention time on the denitrification potential of anaerobically digested swine waste.

Ofon, U. A., Ndubuisi-Nnaji, U. U., Udofia, G. E., Adegoke, A. A., Orji, E. E., Ekaette, M. I., Ukot, C. A., Offiong, N. A. O., Fapojuwo, D. P., & Shaibu, S. E. (2025). Optimization of biogas production with rice straw-derived biochar: Characterization, hormetic effects, and kinetics modelling. *Cleaner Waste Systems, 11*, 100288. https://doi.org/10.1016/j.clwas.2025.100288

Ortega-Castro, J., Herrera-Brunett, G. A., Frey E, C., Oswaldo, J., & Castro, O. (2025). Generation of biogas from solid waste from cattle at the Tunshi Experimental Station. *Journal of Natural Resources Production and Sustainability, 4*(1), 54–74. https://doi.org/10.61236/renpys.v4i1.1020

Pasalari, H., Esrafili, A., Rezaee, A., Gholami, M., & Farzadkia, M. (2021). Electrochemical oxidation pretreatment for enhanced methane potential from landfill leachate in anaerobic co-digestion process: Performance, Gompertz model, and energy assessment. *Chemical Engineering Journal, 422*, 130046. https://doi.org/10.1016/j.cej.2021.130046

Pera, L., Gandiglio, M., Marocco, P., Pumiglia, D., & Santarelli, M. (2024). Trace contaminants in biogas: Biomass sources, variability and implications for technology applications. *Journal of Environmental Chemical Engineering, 12*(6), 114478. https://doi.org/10.1016/j.jece.2024.114478

Petro, L. (2020). *Optimization of domestic biogas stove burner for efficient energy utilization*. https://doi.org/10.58694/20.500.12479/1300

Physics Stack Exchange. (2025). Physics of boiling an egg – What am I missing? (heat capacity and coagulation question). Recuperado de https://physics.stackexchange.com/questions/243496/physics-of-boiling-an-egg-what-am-i-missing-heat-capacity-and-coagulation-qu

Pilarski, G., Kyncl, M., Stegenta, S., & Piechota, G. (2020). Emission of biogas from sewage sludge in psychrophilic conditions. *Waste and Biomass Valorization, 11*(7), 3579–3592. https://doi.org/10.1007/s12649-019-00707-9

Poveda, G., Espinoza, J. C., Zuluaga, M. D., Solman, S. A., Garreaud, R., & van Oevelen, P. J. (2020). High impact weather events in the Andes. *Frontiers in Earth Science, 8*, 162. https://doi.org/10.3389/feart.2020.00162

Rajendran, K., Aslanzadeh, S., & Taherzadeh, M. J. (2012). Household biogas digesters—A review. *Energies, 5*(8), 2911–2942. https://doi.org/10.3390/en5082911

Ramaiyulis, U., Mohtar Lutfi, R., Hendriani, R., & Nefri, J. (2021). Biogas installations for harvesting energy and utilization of natural fertilisers. *International Journal of Scientific & Technology Research, 10*(1), 1–14. https://doi.org/10.1515/agriceng-2020-0001

Rascón, J., Gosgot Angeles, W., Quiñones Huatangari, L., Oliva, M., & Barrena Gurbillón, M. Á. (2021). Dry and wet events in Andean populations of northern Peru: A case study of Chachapoyas, Peru. *Frontiers in Environmental Science, 9*, 614438. https://doi.org/10.3389/fenvs.2021.614438

Ravikumar, D., Hoysall, C. N., & Dasappa, S. (2020). Predicting biomethanation pattern from feedstock composition for biomass residues. En *Bioresource utilization and bioprocess* (pp. 75–79). https://doi.org/10.1007/978-981-15-1607-8_8

Riau, V., De la Rubia, M. Á., & Pérez, M. (2010). Temperature-phased anaerobic digestion (TPAD) to obtain class A biosolids: A semi-continuous study. *Bioresource Technology, 101*(8), 2706–2712. https://doi.org/10.1016/j.biortech.2009.11.101

Rivas-Solano, O., Faith-Vargas, M., & Guillén-Watson, R. (2016). Biodigesters: Chemical, physical and biological factors related to their productivity. *Revista Tecnología en Marcha, 29*(5), 47–53. https://doi.org/10.18845/tm.v29i5.2516

Rodríguez-Jiménez, L. M., Pérez-Vidal, A., & Torres-Lozada, P. (2022). Research trends and strategies for the improvement of anaerobic digestion of food waste in psychrophilic temperature conditions. *Heliyon, 8*(10), e11174. https://doi.org/10.1016/j.heliyon.2022.e11174

SENAMHI. (2025). Chachapoyas weather forecast. Recuperado de https://www.senamhi.gob.pe/?p=pronostico-detalle&dp=01&localidad=0012

Shinde, S., Mangate, L., Gokhale, D., Dongardive, S., Dugge, A., Gaikwad, S., & Garware, P. (2024). Domesticating biogas – A viable alternative to LPG in India. *International Research Journal on Advanced Engineering and Management (IRJAEM), 2*(05), 1353–1360. https://doi.org/10.47392/irjaem.2024.0186

Song, Y., Qiao, W., Westerholm, M., Huang, G., Taherzadeh, M. J., & Dong, R. (2023). Microbiological and technological insights on anaerobic digestion of animal manure: A review. *Fermentation, 9*(5), 436. https://doi.org/10.3390/fermentation9050436

Swinbourn, R., Li, C., & Wang, F. (2024). A comprehensive review on biomethane production from biogas separation and its techno-economic assessments. *ChemSusChem, 17*(19), e202400779. https://doi.org/10.1002/cssc.202400779

Tian, P., Gong, B., Bi, K., Liu, Y., Ma, J., Wang, X., Ouyang, Z., & Cui, X. (2023). Anaerobic co-digestion of pig manure and rice straw: Optimization of process parameters for enhancing biogas production and system stability. *International Journal of Environmental Research and Public Health, 20*(1), 804. https://doi.org/10.3390/ijerph20010804

Tiwari, B. R., Rouissi, T., Brar, S. K., & Surampalli, R. Y. (2021). Critical insights into psychrophilic anaerobic digestion: Novel strategies for improving biogas production. *Waste Management, 131*, 513–526. https://doi.org/10.1016/j.wasman.2021.07.002

Wu, J., Zhang, H., Zhao, Y., Yuan, X., & Cui, Z. (2023). Characteristics of biogas production activity and microbial community during sub-moderate temperature anaerobic digestion of wastewater. *Fermentation, 9*(10). https://doi.org/10.3390/fermentation9100903

Xu, Z., & Chang, L. (2017). *Identification and control of common weeds: Volume 3* (Vol. 3, pp. 1–944). https://doi.org/10.1007/978-981-10-5403-7

Zhang, B., Liu, J., Cai, C., & Zhou, Y. (2025). Membrane photobioreactor for biogas capture and conversion – Enhanced microbial interaction in biofilm. *Bioresource Technology, 418*, 131999. https://doi.org/10.1016/j.biortech.2024.131999

Production of VFAs through anaerobic digestion of cattle and swine manure

Andres Castro-Sierra [1,*], María Myrna Solís-Oba [1], Teodoro Espinosa-Solares [2,3], Eric Houbron [4], José Agustín Pacheco-Ortiz [1], Brenda Yanin Azcárraga-Salinas [1], Javier Ruiz-Romero [1]

[1] Centro de Investigación en Biotecnología Aplicada, Instituto Politécnico Nacional, Tepetitla de Lardizábal, Tlaxcala, México
[2] Agricultural Research and Extension Center, Southern University, Baton Rouge, Luisiana, United States of America
[3] Departamento de Ingeniería Agroindustrial, Universidad Autónoma de Chapingo, Texcoco, Estado de México, México
[4] Facultad de Ciencias Químicas, Universidad Veracruzana, Orizaba, Veracruz, México
* Autor de correspondencia: andres.castro.sierra21@gmail.com

Received: May 27, 2025 Accepted: July 21, 2025 Published: December 16, 2025
DOI: https://doi.org/10.56845/rebs.v7i2.655

Abstract: Anaerobic digestion (AD) is a key biotechnological process for the valorization of organic residues, as it reduces their pollutant load and generates valuable products such as volatile fatty acids (VFAs). These compounds have industrial applications as precursors for biopolymers, solvents, and biofuels. In this study, the kinetics of VFAs were evaluated using cattle manure (CM) and swine manure (SM), incubated at 37 °C for 18 days. A completely randomized design was applied with ten sampling times and three replicates per treatment. VFA quantification was performed by HPLC, and parameters such as chemical oxygen demand (COD), pH, and nutrient concentrations (N, P, K) were also analyzed. SM reached a maximum production of 1.699 g/L at day 4, whereas CM peaked at 1.817 g/L on day 10. In both substrates, pH exhibited an initial decline, indicating hydrolytic and acidogenic phases, followed by stabilization toward acetogenic and methanogenic stages. Reductions in COD, nitrogen, and phosphorus were also observed, reflecting intense microbial activity. Both manures proved viable, with SM being more efficient at early stages and CM performing better in later phases. These findings provide key information for the design of biorefineries within circular economy frameworks.

Keywords: valorization of waste, acidogenic fermentation, environmental biotechnology

Introduction

Anaerobic digestion (AD) is a widely studied biological process due to its relevance in the sustainable management of organic waste and the production of renewable energy. This process is based on the synergistic activity of microbial consortia that, in the absence of oxygen, transform organic matter into metabolic products such as biogas and valuable intermediate compounds. Its application has expanded globally due to its capacity to reduce the pollutant load of agro-industrial residues, mitigate greenhouse gas emissions, and replace fossil-based energy sources, aligning with the principles of environmental sustainability and the circular economy (Atelge *et al*., 2020).

The AD mechanism consists of four interdependent microbial stages: hydrolysis, acidogenesis, acetogenesis, and methanogenesis. During hydrolysis, specialized bacteria degrade complex polymers (such as cellulose, hemicellulose, proteins, and lipids) into soluble monomers. Then, in acidogenesis, these products are fermented into simpler compounds, including volatile fatty acids (VFAs), ethanol, lactate, carbon dioxide (CO_2), and hydrogen gas (H_2). Acetogenesis converts these intermediates into acetate, H_2, and CO_2, and finally, during methanogenesis, methanogenic archaea utilize these compounds to generate methane (CH_4), the main energy component of biogas (Giduthuri & Ahring, 2023; Patel *et al*., 2021).

Within these stages, VFA production is strategically important not only as an intermediate step on the pathway to CH_4 formation but also as an alternative route for obtaining value-added compounds. VFAs—including acetic, formic, propionic, isobutyric, butyric, isovaleric, valeric, isocaproic, caproic, and enanthic acids—are low-molecular-weight molecules which can serve as raw materials for the manufacture of biopolymers, solvents, biofuels, food supplements, and chemical additives (Franke-Whittle *et al*., 2014; Harirchi *et al*., 2022). This dual functionality, as both metabolic intermediates and final products, has motivated the development of anaerobic digestion systems specifically oriented toward maximizing their accumulation rather than favoring methanogenesis.

The efficiency and selectivity of the process depend on multiple operational factors such as temperature, pH, digestion time, and critically the type of substrate used. In this context, livestock manures, particularly cattle and swine manure, represent abundant and economically accessible sources of fermentable organic matter. Their nutrient-rich composition, high nitrogen content, and elevated proportion of volatile solids make them ideal candidates for

acidogenic fermentation. However, physicochemical differences between these substrates can influence microbial dynamics, the predominant metabolic pathway, and the VFA accumulation rate (Cisneros De La Cueva *et al*., 2021; Wang *et al.,* 2022).

From this perspective, the present study aims to evaluate VFA production during the anaerobic digestion of cattle and swine manure at a constant temperature of 37 °C. To achieve this, different digestion times (0, 2, 4, 6, 8, 10, 12, 14, 16, and 18 days) were established, allowing for a detailed kinetic analysis of the fermentative behavior of each substrate. This evaluation not only enabled comparison of VFA yield, production, and composition between the two manures but also provided key information for optimizing anaerobic systems oriented toward the generation of industrially valuable biocompounds.

Materials and Methods

Cattle manure (CM) and swine manure (SM) samples were collected in Tlaxcala, Mexico. CM had an initial dry matter content of 22.41% and a pH of 8.02, whereas SM exhibited 29.09% dry matter and a pH of 6.15. The samples were subjected to air-drying at ambient temperature (25 ± 5 °C), followed by homogenization by manual grinding in a mortar and subsequent sieving through a MONTINOX No. 20 mesh. Once processed, the samples were stored in sealed glass jars under dark and dry conditions until use.

Experimental design

To evaluate VFA production, a completely randomized design (CRD) was implemented, considering two main factors: substrate type (CM and SM) and digestion time (0, 2, 4, 6, 8, 10, 12, 14, 16, and 18 days), at a constant temperature of 37 °C, with three replicates per treatment, resulting in a total of 60 experimental units. The experiment was conducted in batches using 600-mL glass flasks as reactors, each loaded with 5% substrate (CM or SM), 5% (v/v) inoculum obtained from a previous anaerobic digestion process (Castro-Sierra *et al*., 2024), and distilled water to reach a final working volume of 500 mL. The flasks were purged with N_2 to remove residual oxygen and then hermetically sealed. Incubation was carried out in an ECOSHEL 9165 unit for 18 days, with periodic monitoring every two days.

Physicochemical evaluation of the digestates

The digestates obtained during the anaerobic digestion process were characterized through a comprehensive analysis of their physicochemical properties. The evaluated variables included chemical oxygen demand (COD) and the concentrations of total nitrogen (N), total phosphorus (P), and total potassium (K), which were determined using HACH analysis kits and a HACH DR 2800 spectrophotometer. Moisture content was measured with an OHAUS MB45 thermobalance, while total solids (TS) and volatile solids (VS) were quantified by calcination in a THERMOLYNE 1400 muffle furnace. pH was measured using a HINOTEK PHS-3E potentiometer. All determinations were performed following the standardized protocols in the Standard Methods for the Examination of Water and Wastewater of the APHA (2017).

Determination of total volatile fatty acid (VFAs) production

The digestates were centrifuged at 9000 rpm for 10 minutes at 20 °C using a LABNET PRISM R refrigerated microcentrifuge. Subsequently, 2 mL of the supernatant was collected and filtered through 0.22 µm CORNING syringe filters. The identification and quantification of volatile fatty acids (VFAs) were performed by high-performance liquid chromatography (HPLC) using an Agilent 1100 G1311A system coupled to a REZEX ROA-ORGANIC ACID H^+ (8%) ion-exclusion column. The analysis was conducted under isocratic flow conditions, employing HPLC-grade water acidified with 0.005 M sulfuric acid as the mobile phase, at a flow rate of 0.6 mL/min for a total runtime of 30 minutes. Detection was carried out at 205 nm, with the column maintained at a constant temperature of 65 °C (Colzi & Estrada, 2020; Tabarez *et al*., 2024).

VFAs quantification was based on calibration curves generated from a Sigma-Aldrich reference standard mixture containing the following compounds: acetic acid (99.90% purity), formic acid (98.30%), propionic acid (99.70%),

isobutyric acid (99.90%), butyric acid (99.90%), isovaleric acid (100.00%), valeric acid (99.90%), isocaproic acid (99.80%), caproic acid (99.60%), and enanthic acid (99.70%). All standard solutions had certified concentrations of 10.0 ± 0.2 mM.

Results and Discussion

Organic matter and nutrients

Figure 1 shows the kinetics of chemical oxygen demand (A), nitrogen (B), phosphorus (C), and potassium (D) during the anaerobic digestion (AD) of cattle and swine manure at 37 °C. With both substrates, COD showed a progressive decrease (a total reduction of 18.2% in cattle manure and 20.8% in swine manure) throughout the process. Approximately 10% of COD in an anaerobic process is used for biomass synthesis, so its reduction indicates microbial activity during digestion (González & Jurado, 2017). Additionally, this significant decrease reflects effective degradation of easily biodegradable organic matter, which serves as the basis for VFA production (Meegoda *et al*., 2018). Cattle manure maintained higher COD values for a longer period, suggesting a higher content of recalcitrant compounds or slower degradation rate. In contrast, swine manure exhibited a faster COD reduction due to its higher content of readily biodegradable compounds (Lee *et al*., 2023).

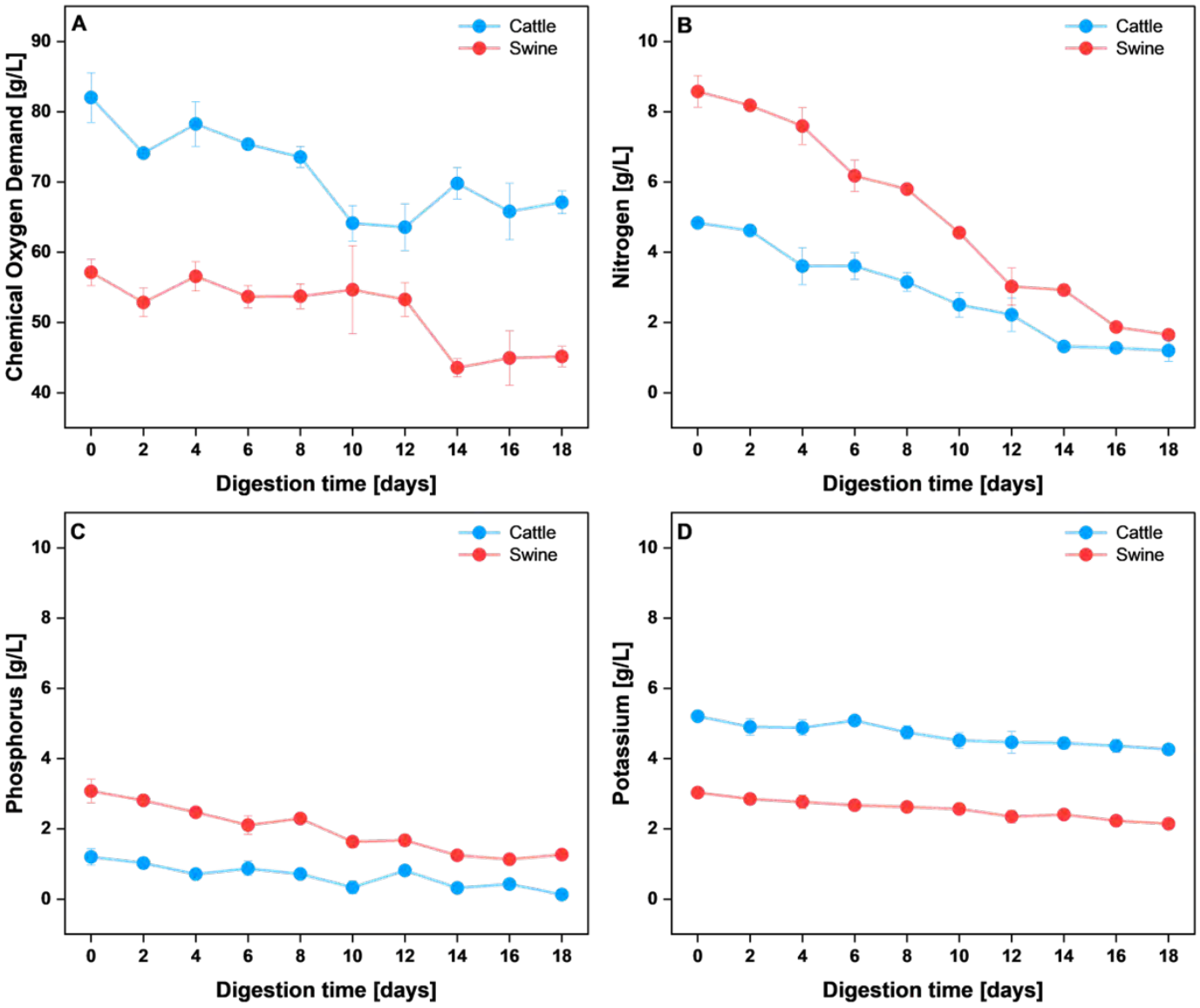

Figure 1. Kinetics of chemical oxygen demand (A), nitrogen (B), phosphorus (C), and potassium (D) during the anaerobic digestion of cattle and swine manure

Similarly, nitrogen exhibited a general decreasing trend (total reduction of 75.0% for cattle manure and 80.2% for swine manure). During AD, nitrogen decreases due to its conversion into gaseous forms such as ammonia (NH_3) and due to microbial assimilation (Kadam *et al*., 2024). The reduction was more pronounced in swine manure, likely attributable to its higher content of soluble proteins, which are more susceptible to ammonification.

Phosphorus also exhibited a continuous decline in both treatments (total change of 91.7% in cattle manure and 58.1% in swine manure), with a greater reduction in cattle manure. This decrease is associated with its incorporation into microbial biomass and the precipitation of insoluble phosphates. Given the magnitude and consistency of this behavior in both substrates, which aligns with recent studies, phosphorus not consumed could potentially be recovered through electrochemical methods (Chen *et al*., 2023).

Unlike the other nutrients, potassium remained relatively stable, with only slight decreases in both manures (17.3% in cattle manure and 30.0% in swine manure). This is because potassium is a mobile element, does not directly participate in microbial transformation reactions, and is mainly present in soluble ionic form. Its slight decrease may be due to incorporation into microbial biomass or minimal losses through leaching. This behavior is consistent with studies reporting the stability of K during anaerobic processes (Tambone *et al*., 2009).

pH and volatile fatty acids

During anaerobic digestion (AD), the pH of both substrates exhibited a pronounced initial decrease (Figure 2, panel A). In the case of swine manure, the initial pH was alkaline (8.96) compared to cattle manure (7.81), but both shifted toward acidic values during the first 4 days, reaching minimums of 6.40 and 5.86, respectively. This corresponds to an intense acidogenic phase, in which the production of volatile fatty acids (VFAs) lowers the pH of the medium (Anukam *et al*., 2019). Subsequently, stabilization was observed in both treatments, with slight fluctuations. The pH of the cattle digestate remained lower throughout the entire period, whereas the swine digestate maintained consistently higher values after day 4, likely indicating lower acid accumulation or better buffering of the organic acids produced. This may be attributed to natural buffering systems such as carbonates and ammonium present in this manure (González-Herrera *et al*., 2021; Solarte *et al*., 2017).

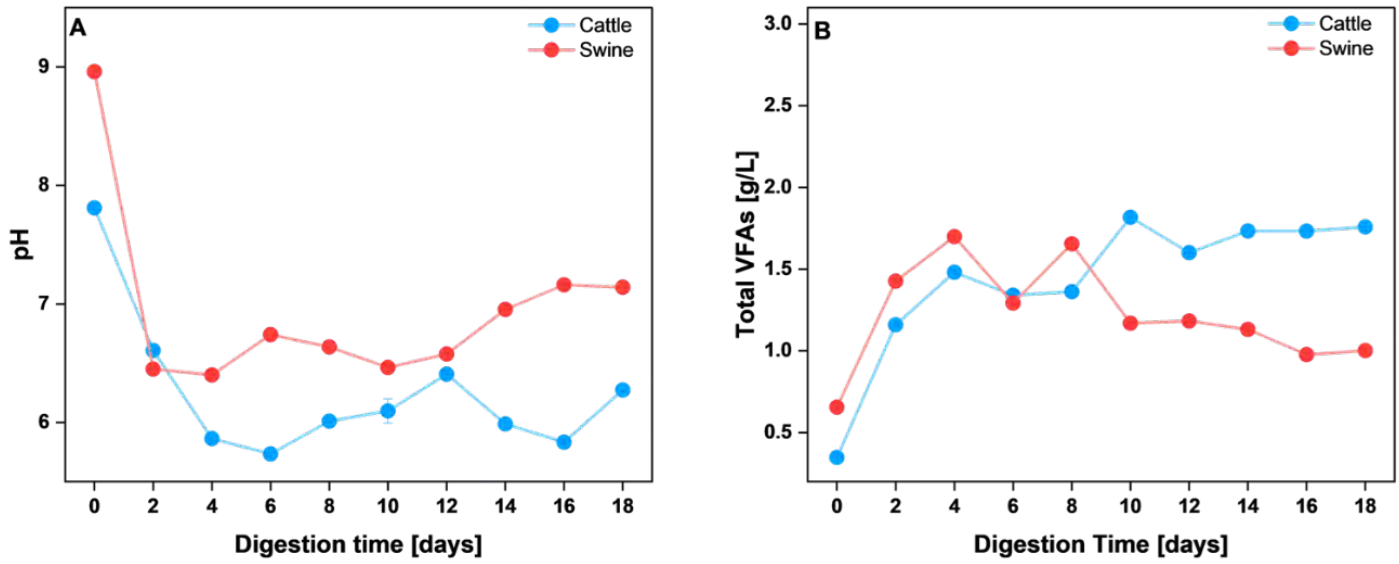

Figure 2. Changes in pH and VFAs production kinetics during the anaerobic digestion of cattle and swine manure

Regarding VFAs production (Figure 2, panel B), both digestates show a sustained increase during the first days of the process. Swine manure exhibits a higher initial VFA production, rising from 0.655 g/L to 1.699 g/L between days 0 and 4, suggesting high availability of fermentable compounds and an active acidogenic microbiota, consistent with its higher content of soluble proteins and lipids (Risberg *et al*., 2017). In contrast, cattle digestate increases more gradually, reaching 1.480 g/L on day 4, but continues rising until reaching its absolute maximum on day 10 with 1.817 g/L. This

indicates a slower fermentation kinetics, likely attributable to a matrix with a higher proportion of structural fiber and lower content of easily accessible solutes.

This behavior highlights substantial differences in fermentative dynamics between the two substrates. While swine manure favors early and intense VFA production that stabilizes after day 8, cattle manure maintains sustained and progressive production into later stages, which may be associated with slower hydrolysis of its complex organic components (Bajpai, 2017).

In both cases, the initial decrease in pH correlates with the increase in VFAs, particularly between days 0 and 4. Swine digestate shows a faster pH recovery after the acidic peak, possibly due to a higher buffering capacity or an earlier onset of the methanogenic phase. Conversely, cattle digestate maintains a lower pH over time, which may reflect slower conversion of VFAs to methane or sustained acid accumulation that inhibits methanogenic microorganisms (Castro-Ramos *et al*., 2022).

Conclusions

The results support the use of swine manure (SM) as an ideal substrate for rapid and intensive production of volatile fatty acids (VFAs), whereas cattle manure (CM) may be better suited for prolonged fermentation strategies. SM showed higher efficiency in early VFA accumulation, reaching values up to 1.699 g/L between days 0 and 4, and remaining elevated until day 8. This behavior reflects accelerated acidogenesis, attributable to the greater availability of fermentable substrates. In contrast, CM reached its maximum VFA concentration on day 10 (1.817 g/L), indicating a slower but steady acidogenic kinetics throughout the process. This result suggests that CM may have greater accumulation potential during intermediate stages, likely associated with the gradual release of complex organic compounds.

Acknowledgments and Funding: To CIBA-IPN, FCQ-UV, and UACh for the support provided during this research. To SECIHTI for the scholarship awarded (No. 966741), and to the “Secretaría de Investigación y Posgrado” for supporting project SIP 20220594.

Author contributions: A.C.-S.: conceptualization, experimental design, data analysis and interpretation, writing and editing of the manuscript; M.M.S.-O.: supervision, project administration and critical revision; T.E.-S.: methodological contribution, data analysis and editing; E.H.: technical advising and manuscript revision; J.A.P.-O.: support in experimental design, data collection and validation; B.Y.A.-S.: sample processing, laboratory analysis and data curation; J.R.-R.: statistical analysis support, editing and visualization of results.

References

American Public Health Association, American Water Works Association, & Water Environment Federation. (2017). *Standard methods for the examination of water and wastewater* (L. L. Bridgewater, R. B. Baird, A. D. Eaton, & E. W. Rice, Eds.; 23rd ed.). American Public Health Association.

Anukam, A., Mohammadi, A., Naqvi, M., & Granström, K. (2019). A review of the chemistry of anaerobic digestion: Methods of accelerating and optimizing process efficiency. *Processes, 7*(8), Article 8. https://doi.org/10.3390/pr7080504

Atelge, M. R., Krisa, D., Kumar, G., Eskicioglu, C., Nguyen, D. D., Chang, S. W., Atabani, A. E., Al-Muhtaseb, A. H., & Unalan, S. (2020). Biogas production from organic waste: Recent progress and perspectives. *Waste and Biomass Valorization, 11*(3), 1019–1040. https://doi.org/10.1007/s12649-018-00546-0

Bajpai, P. (2017). Basics of anaerobic digestion process. En *Anaerobic technology in pulp and paper industry* (pp. 7–12). Springer. https://doi.org/10.1007/978-981-10-4130-3_2

Castro-Ramos, J. J., Solís-Oba, A., Solís-Oba, M., Calderón-Vázquez, C. L., Higuera-Rubio, J. M., & Castro-Rivera, R. (2022). Effect of the initial pH on the anaerobic digestion process of dairy cattle manure. *AMB Express, 12*(1), 162. https://doi.org/10.1186/s13568-022-01486-8

Castro-Sierra, A., Espinosa-Solares, T., Houbron, E., Castro-Rivera, R., & Azcárraga-Salinas, B. Y. (2024). Production of phytoregulators during anaerobic digestion of bovine and swine manures. *Revista Mexicana de Ingeniería Química, 23*(3). https://doi.org/10.24275/rmiq/Bio24289

Chen, T., Song, X., & Xing, M. (2023). Study on anaerobic phosphorus release from pig manure and phosphorus recovery by vivianite method. *Scientific Reports, 13*(1), 16095. https://doi.org/10.1038/s41598-023-43216-5

Cisneros De La Cueva, S., Veana Hernández, F., Arjona López, M. A., Álvarez Guzmán, C. L., & Pérez Vega, S. B. (2021). Optimización de las variables del proceso de digestión anaerobia de lactosuero en la producción de biogás. *Revista Internacional de Contaminación Ambiental*. https://doi.org/10.20937/RICA.53879

Colzi, A., & Estrada, J. (2020). Producción de ácidos grasos volátiles a partir de fangos de depuradora. *AQUAVALL*. Recuperado de https://aquavall.es/wp-content/uploads/2020/07/Apuntes-de-Innovacion-AquaVall-01-Produccion-de-acidos-grasos-TROVANT-web.pdf

Franke-Whittle, I. H., Walter, A., Ebner, C., & Insam, H. (2014). Investigation into the effect of high concentrations of volatile fatty acids in anaerobic digestion on methanogenic communities. *Waste Management, 34*(11), 2080–2089. https://doi.org/10.1016/j.wasman.2014.07.020

Giduthuri, A. T., & Ahring, B. K. (2023). Current status and prospects of valorizing organic waste via arrested anaerobic digestion: Production and separation of volatile fatty acids. *Fermentation, 9*(1), Article 1. https://doi.org/10.3390/fermentation9010013

González, E. T., & Jurado, P. C. (2017). Sustratos y producción de biogás en biodigestores: Una revisión sistemática. *Ingeciencia, 2*(1), Article 1. Recuperado de https://revistas.ucentral.edu.co/index.php/Ingeciencia/article/view/2352

González-Herrera, J. E., Hernández-Beltrán, Y., González, L. M. L., & Hernández, J. J. (2021). Digestión anaerobia de suero de queso utilizando inóculo de estiércol porcino a diferentes relaciones inóculo-sustrato. *Revista ION, 48*(3).

Harirchi, S., Wainaina, S., Sar, T., Nojoumi, S. A., Parchami, M., Parchami, M., Varjani, S., Khanal, S. K., Wong, J., Awasthi, M. K., & Taherzadeh, M. J. (2022). Microbiological insights into anaerobic digestion for biogas, hydrogen, or volatile fatty acids (VFAs): A review. *Bioengineered, 13*(3), 6521–6557. https://doi.org/10.1080/21655979.2022.2035986

Kadam, R., Jo, S., Lee, J., Khanthong, K., Jang, H., & Park, J. (2024). A review on the anaerobic co-digestion of livestock manures in the context of sustainable waste management. *Energies, 17*(3), Article 3. https://doi.org/10.3390/en17030546

Lee, J.-H., Kim, C.-H., & Yoon, Y.-M. (2023). Effects of hydrothermal pretreatment on methane potential of anaerobic digestion sludge cake of cattle manure containing sawdust as bedding materials. *Animal Bioscience, 36*(5), 818–828. https://doi.org/10.5713/ab.22.0434

Meegoda, J. N., Li, B., Patel, K., & Wang, L. B. (2018). A review of the processes, parameters, and optimization of anaerobic digestion. *International Journal of Environmental Research and Public Health, 15*(10), Article 10. https://doi.org/10.3390/ijerph15102224

Patel, A., Mahboubi, A., Horváth, I. S., Taherzadeh, M. J., Rova, U., Christakopoulos, P., & Matsakas, L. (2021). Volatile fatty acids generated by anaerobic digestion serve as feedstock for oleaginous microorganisms to produce biodiesel and added-value compounds. *Frontiers in Microbiology, 12*. https://doi.org/10.3389/fmicb.2021.614612

Risberg, K., Cederlund, H., Pell, M., Arthurson, V., & Schnürer, A. (2017). Comparative characterization of digestate versus pig slurry and cow manure: Chemical composition and effects on soil microbial activity. *Waste Management, 61*, 529–538. https://doi.org/10.1016/j.wasman.2016.12.016

Solarte Toro, J. C., Mariscal Moreno, J. P., & Aristizábal Zuluaga, B. H. (2017). Evaluación de la digestión y co-digestión anaerobia de residuos de comida y de poda en bioreactores a escala laboratorio. *Revista ION, 30*(1), 105–116. https://doi.org/10.18273/revion.v30n1-2017008

Tabarez Hincapie, K. V., Ramón Vanegas, A. A., Carrasco Salcedo, L. M., & Vásquez Bustamante, J. E. (2024). Evaluación de la producción de biogás a partir de cáscara y mucílago de cacao. *Revista Ambiental Agua, Aire y Suelo, 15*(1), Article 1. https://doi.org/10.24054/raaas.v15i1.2891

Tambone, F., Genevini, P., D'Imporzano, G., & Adani, F. (2009). Assessing amendment properties of digestate by studying the organic matter composition and degree of biological stability during anaerobic digestion of the organic fraction of MSW. *Bioresource Technology, 100*(12), 3140–3142. https://doi.org/10.1016/j.biortech.2009.02.012

Wang, Z., Wang, W., Li, P., Leng, Y., & Wu, J. (2022). Continuous production of volatile fatty acids (VFAs) from swine manure: Determination of process conditions, VFAs composition distribution and fermentation broth availability analysis. *Water, 14*(12), Article 12. https://doi.org/10.3390/w14121935